INCORPORATION OF METAL-ORGANIC FRAMEWORK AND POLYOXOMETALATE WITH FIBROUS MATERIALS AND THEIR EFFECTIVENESS IN REMOVAL AND DEGRADATION OF AN ORGANOPHOSPHATE

A Dissertation

Presented to the Faculty of the Graduate School

of Cornell University

In Partial Fulfillment of the Requirements for the Degree of

Doctor of Philosophy

by

Laura Elizabeth Lange

January 2014

INCORPORATION OF METAL-ORGANIC FRAMEWORK AND POLYOXOMETALATE WITH FIBROUS MATERIALS AND THEIR EFFECTIVENESS IN REMOVAL AND DEGRADATION OF AN ORGANOPHOSPHATE

Laura Elizabeth Lange, Ph. D.
Cornell University 2014

The adsorption and degradation of methyl parathion an organophosphate with Cu-BTC metal-organic framework (MOF-199) and a polyoxometalate are investigated in multiple fibrous systems. Immobilizing MOF particles in a fibrous system adds functionality to the fibers and allows the MOF particles to be in a workable and flexible substrate.

First, a method is presented to immobilize Cu-BTC metal-organic framework (MOF-199) particles by enmeshing them in nonwoven polyacrylonitrile (PAN) nanofibers creating a fibrous membrane with the potential ability to remove chemical warfare agents or pesticides from solution. These membranes were shown to effectively adsorb methyl parathion, an organophosphate pesticide. Based on solubility theory and experimental results, partitioning was determined to be the main mechanism of removal. After 2 hours, the PAN/MOF-199 membranes removed 88% more methyl parathion than the unmodified PAN membranes and 62% as much as the

MOF-199 crystal powder.

Further experiments revealed that degradation of methyl parathion was occurring within the MOF cages. Degradation of methyl parathion adsorbed in metal-organic framework (MOF)-199 cages was studied using nuclear magnetic resonance (NMR), Raman spectrometry, and solvent extractions. NMR was completed using solid-state ^{31}P NMR with magic-angle spinning with cross polarization or direct polarization. Results show that constitutional isomerization is the main mechanism of methyl parathion degradation within the MOF-199 framework within the 5-67 day time frame studied.

Secondly, A combination of a Keggin-type polyoxometalate (POM), $[CuPW_{11}O_{39}]^{5-}$, with a metal-organic framework (MOF), MOF-199 (HKUST-1) was successfully self-assembled on a cellulose substrate (cotton) with a newly developed room-temperature process. This material was found to effectively remove 2.75 times as much of a target organophosphate toxin, methyl parathion, from a hexane solution as MOF-cotton and cotton control samples after 2 h.

The combination of the catalytic activity of the POM and the adsorption properties of the MOF both immobilized on a textile is ideal for potential applications in protective self-decontaminating materials. In addition to this, hydrophilicity of the fabrics is maintained, which leads to a material that maintains the thermal comfort of cotton. The functionalized fibrous PAN/MOF-199 membranes also have potential to be used in protective clothing for occupational or military applications or as filtration media.

BIOGRAPHICAL SKETCH

Laura Elizabeth Lange was born and raised in Farmington Hills, MI, a suburb of Detroit. She graduated from the University of Michigan-Ann Arbor with a Bachelor of Science degree in Chemistry in 2008. There she was a member of the University of Michigan Synchronized Swimming team. In Fall 2008, she began her M.S./Ph.D. in Fiber Science at Cornell University. She received her M.S. in Fiber Science in May 2011. While at Cornell, she was the President of both the Textile and Apparel Journal Club and the Ithaca Underwater Hockey Club.

To all my family and friends for their years of support

ACKNOWLEDGMENTS

I first and foremost, want to thank my advisor, Professor S. Kay Obendorf for her years of guidance and support. I would also like to thank my committee members: Professor Juan P. Hinestroza, Professor Ann T. Lemley, and Professor Geoffrey W. Coates for their time and contribution to this dissertation. Professor Hinestroza and Fredrick O. Ochanda are additional co-authors of the published version of Chapter 1, and I would like to thank them both for this collaboration. Fredrick O. Ochanda made the fiber mats developed for Chapter 1. Special thanks to Ivan Keresztes of the Cornell University NMR Facility in the Department of Chemistry and Chemical Biology for his expertise in conducting ^{31}P Solid state NMR experiments for Chapter 2. Prof. Christopher Umbach and Leah McEwen were extremely helpful in the operation of the Raman spectrometer and Raman spectra interpretation required for Chapter 2. Craig Hill and Zhen Luo are acknowledged for providing the polyoxometalate: $K_5[CuPW_{11}O_{39}]$, without their contribution, the work completed for Chapter 3 would not be possible.

I want to thank my fellow lab mates: Nancy Elizabeth Allen, Yunfei Han, Mark Chan, and Dong Jin Woo for all of their help and ideas in group meeting, lab, and the office. I also would like to thanks my other fellow fiber science graduate students who have been there for me throughout my time at Cornell: Soshana Smith, Robert (Sandy) Flint, Erin Hendrick Kirkpatrick, Mary Guerra, and Thomas Ellingham.

This dissertation research was funded through grants from the Cornell

Agricultural Experiment Station, North Central Regional Research Project NC 170 federal formula funds, Project NYC329801 received from Cooperative State Research, Education, and Extension Service, U.S. Department of Agriculture; Department of Fiber Science & Apparel Design; College of Human Ecology; American Association of Textile Chemists and Colorists; and the Defense Threat Reduction Agency through the Department of Defense (Subaward No. 8980 G KB786). This work made use of the Cornell Center for Materials Research Shared Facilities, which are supported through the NSF MRSEC program (DMR-1120296).

TABLE OF CONTENTS

LIST OF FIGURES

LIST OF TABLES

LIST OF SCHEMES

CHAPTER 1

INTRODUCTION

1.1. Protective Materials Background

There is a significant need for research targeting the issues with current agricultural and military personal protection equipment (PPE). Some chemical PPE systems currently used involve impermeable barriers. These barrier materials are typically uncomfortable because as the material blocks the passage of dangerous chemicals, it also blocks water vapor and air from flowing across the material. Therefore, barriers materials result in uncomfortable clothing in which to work, especially in the conditions that many agricultural workers and military personnel are exposed to in the field. To address these issues, semi-permeable materials have been developed. However, due to the cost of semi-permeable PPE, many agricultural workers tend to use less chemical resistant, but more comfortable work attire.

PPE is necessary because some pesticides pose a danger for agricultural workers through inhalation, ingestion, and notably dermal absorption. Due to the possibility of dermal adsorption, the families of agricultural workers have an increased risk of exposure to pesticides from contaminated clothing entering the home. It is estimated by the EPA that in the United States there are 10,000-20,000 confirmed pesticide poisonings each year out of among about two million agricultural workers[1]. Similarly, chemical warfare agents pose a danger to military personnel through the same exposure routes and have similar biological effects in humans as pesticides.

A possible solution to increase the functionality and comfort of PPE is to

incorporate an adsorbent and/or catalytic material in the fibers of a microporous membrane or a conventional fabric. These materials have the potential to be used in a layered fibrous system for improved comfort while providing protection from toxins. The catalytic materials would have the ability to degrade pesticides, resulting in a self-decontaminating fibrous material, while the adsorbent material could be used to retain any toxic degradation products or unaltered starting compound. This type of material could have the capacity to breathe like a conventional fabric, but would still possess the necessary protection for agricultural workers or military personnel.

In the literature there have been a variety of compounds that are either very good adsorbents or good oxidative catalysts. Recently, metal organic frameworks (MOFs) have been developed. They are of wide interest for use as adsorbents due to their large surface areas and controllable pore sizes. More interestingly, MOFs have been shown to have an increased potential for selectively adsorbing chemicals and gases[2,3,4], which could be extremely beneficial for applications in comfortable protective clothing. Specifically, MOF-199 shows framework activity in the form of Lewis acid catalytic activity that is related to open metal sites in the Cu(II) coordination sphere[5] indicating potential for accelerated degradation of a test toxins when in the presence of the MOF-199 structure.

In addition to the open Cu(II) metal sites in MOF-199, there is potential for encapsulation of other active agents into the cages of the MOFs. Polyoxometalates (POMs) are a class of materials that has recently been incorporated into MOFs. With regard to chemical threats such as chemical and biological warfare agents, POMs are very promising materials for oxidative self-decontamination. POM catalysts are

regenerated by oxygen in ambient air following oxidation of a threat compound, ideally to a less toxic compound[6,7]. A class of POMs that is particularly useful in air-based oxidations is polytungstates containing 3d metals, such as Cu, substituted at the surface positions[8-12]. There have been multiple reports of encapsulating POMs within the cage structure of the MOF[6, 13-22]. Some of these efforts resulted in materials that possessed the selective adsorption of the MOF with the catalytic activity of the POM.

With regard to protective clothing or textiles, the benefit of combining MOF and POM materials on a textile fabric, not only improves the catalytic self-decontaminating properties of the textile by incorporating the POM, but also allows for possible adsorption of potentially harmful oxidation products by incorporation of the MOF structure[7] to create a multifunctional material with potential applications in protective clothing.

1.2. Abridged Test Toxin Toxicological Profile - Methyl Parathion

1.2.1. Methyl Parathion Overview

One significant class of pesticides and chemical warfare agents is organophosphates, which act as nerve agents. Organophosphates and other nerve agents, such as methyl parathion, inhibit the acetylcholinesterase enzyme by blocking the binding site, preventing acetylcholine from degrading[23,24]. Organophosphate pesticides, organophosphate chemical warfare agents, and acetylcholine have similar structures[24]. When the acetylcholinesterase enzyme binding sites are blocked, high levels of acetylcholine result, leading to possible death from asphyxiation. Aside from the neurotoxic effects, methyl parathion is also toxic to several organs, such as the liver, cardiovascular, and muscular systems[25]. Additionally, methyl parathion

exposure can lead to lowered concentration, slower information processing time, memory and speech impairment, depression, and anxiety[26].

Out of the over 20,000 pesticide products used in the United States[1], methyl parathion was chosen for this research for multiple reasons. First of all, methyl parathion can act as a mimic for more harmful organophosphates that are used as chemical warfare agents. Secondly, even though it is still used as an agricultural pesticide in the U.S. and other areas abroad, it can cause severe poisoning effects in humans. Methyl parathion is considered to have an extremely hazardous (Class IA) toxicity according to the World Health Organization[27].

Methyl parathion is an organophosphate used as an agricultural insecticide. Over the years, the amount of methyl parathion used in the United States has varied significantly. In 1966, 8,002,000 lbs/year were used in the US. This number increased significantly to 27,563,000 lbs/year in 1971 and 23,350,000 in 1976[28]. In 1978, the use of methyl parathion was restricted in the United States to be applied only by a certified individual as an agricultural insecticide[29].

1.2.2. Physical Characteristics

Methyl parathion is classified as an organophosphate, and its chemical name is O,O-dimethyl O-4-nitrophenyl phosphorothioate. Its molecular weight is 263.23 g/mol[30]. Methyl parathion's chemical formula is $C_8H_{10}NO_5PS$ with the chemical structure seen in Figure 1.1. Some physical properties of methyl parathion include a vapor pressure at 25-35 ˚C of 0.41mPa and a melting point of 35-36 ˚C[31]. Methyl parathion decomposes at 120 ºC before it reaches its boiling point[32]. The water solubility is 50 ppm[30] and it is soluble in a variety of organic solvents like ethanol,

chloroform, aromatic and aliphatic solvents[33]. While the half life of methyl parathion in water at pH 8 has been reported as 119 days[34], degradation of methyl parathion is dependent on temperature and pH and it has been shown that at higher temperatures and higher pHs, methyl parathion degrades quicker. In humans, methyl parathion is quickly metabolized and excreted.

1.2.3. Environmental Fate

In water, methyl parathion degradation occurs by way of biotransformation, hydrolysis, photolysis, and volatilization. In general these degradation reactions occur quite quickly. Figure 1.2 shows a proposed set of degradation pathways for methyl parathion in water. Methyl parathion degrades at different rates in water depending upon pH. The rate of methyl parathion degradation increases in water with increasing pH and temperature. Introducing a catalyst also helps facilitate degradation of methyl parathion. Using TiO_2, another metal oxide degradation catalyst, the degradation pathway in Figure 1.3 was observed[35]. This pathway represents a small subset of the degradation reactions seen in Figure 1.2.

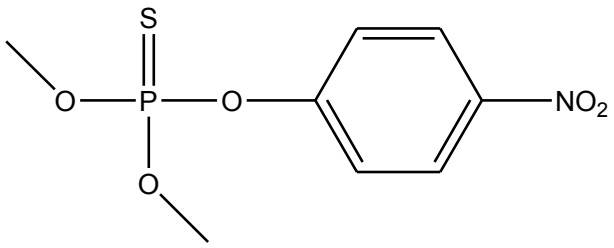

Figure 1.1. Methyl parathion chemical structure.

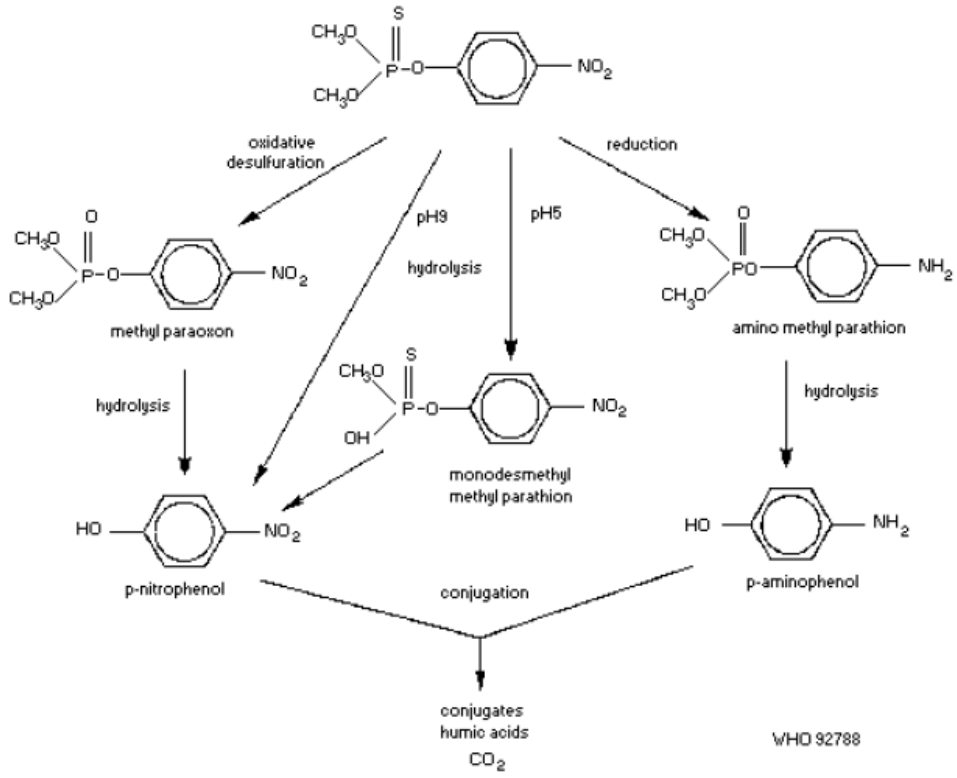

Figure 1.2. Proposed degradation pathways for methyl parathion in aqueous systems[36].

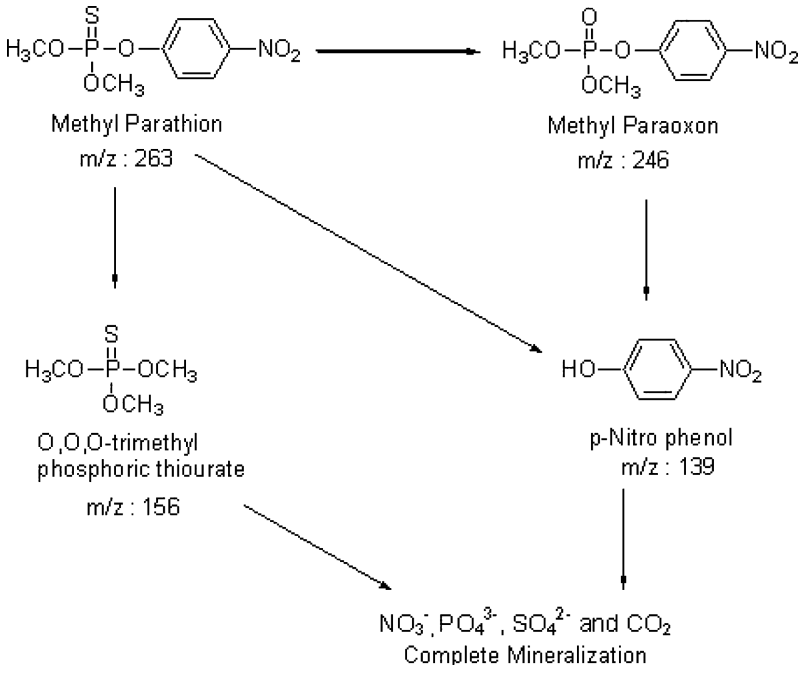

Figure 1.3. Possible degradation pathway of methyl parathion in coated TiO_2[35].

Methyl parathion degradation in sediments and soils relies largely upon hydrolysis and biodegradation (more so in anaerobic soil than aerobic) [37,38], but not as much upon photolysis[39]. Also, it was found that in moist soils, methyl parathion residues bound to the surface of those soils and that 4-nitrophenol and 4-aminophenol were the main degradation products and biodegrade to CO_2[37,40], which is also seen in Figure 1.2 and Figure 1.3. Overall in soil, methyl parathion degrades faster with more alkaline pH[37], higher temperatures[41], and higher moisture content[37,38]. It was determined that not very much methyl parathion leaches into the groundwater or volatizes after entering the soil[42,43]. The log K_{ow} for methyl parathion is 2.86[44], which in combination with the low solubility of 50-60 ppm[30] would suggest that methyl parathion is more likely to adsorb onto soil or other organic matter as opposed to water. This could also be related to how methyl parathion is adsorbed by metal organic frameworks.

1.2.4. Exposure

Humans can be exposed by contamination through absorption through the skin, ingestion, and inhalation. In experiments done on rats, it was shown that there is a difference in the effects of a single dermal exposure to methyl parathion of a dose lower than the amount that results in small toxic symptoms and a repeated skin absorbed exposure of a low dose of methyl parathion. The single exposure can cause reversible inhibition of blood cholinesterase and changes in motor function. The repeated exposure was shown to maintain the inhibition of blood cholinesterase, impaired motor function, and also impaired memory retention[45].

It is difficult to ethically study the effects of methyl parathion exposure in

humans, so individual case studies are typically reported in the literature. In one study, it was found that the animal testing may not be a good predictor of methyl parathion toxicity in humans[46]. These researchers concluded that it would take more than a mouthful or two of methyl parathion for a human to sustain severe negative poisoning effects from oral exposure, despite what was found in previous animal studies[46]. Methyl paraoxon, a main metabolite of methyl parathion, is at least ten times more toxic than methyl parathion[47]. This means that even if methyl parathion degrades to methyl paraoxon, the toxicity danger to humans is still present until more complete degradation takes place.

1.3. Objectives

This research will detail three related but different projects including: (1) A method of incorporating a metal organic framework into a polyacrylonitrile (PAN) microfibrous membrane and the characterization of the adsorption of a test toxin, methyl parathion, by this material, (2) An investigation of test toxin degradation within the pores of the metal organic framework from the first project, (3) room temperature method of growing a multiunit polyoxometalate – metal organic framework oxidative catalyst and adsorbent material and its removal of a test toxin. These three projects lead to the development of a comfortable self-decontaminating fabric that has the ability to adsorb degradation products as well.

It is proposed that, due to the selective adsorption and potential catalytic properties of MOF-199, enmeshing MOF-199 into an electrospun fibrous membrane will result in an immobilized adsorbent with potential self-decontaminating properties. The objectives are to create these membranes, characterized them, and evaluate their

performance by using a test toxin. Performance is evaluated based on how long the membranes take to adsorb the toxin as well how much toxin they remove in comparison to a control sample.

Next, it was important to evaluate the self-decontaminating properties of these materials. The easiest way to do this was to work directly with the MOF-199 particles not enmeshed in the fibrous membrane. As mentioned previously, it is suspected that degradation of methyl parathion is occurring within the cages of the MOF-199 because MOF-199 shows framework activity in the form of Lewis acid catalytic activity that is related to open metal sites in the Cu(II) coordination sphere[5]. Aiming to confirm and characterize the degradation of the test toxin within the MOF-199 pores, a combination of solid-state ^{31}P nuclear magnetic resonance (NMR), Raman spectroscopy and solvent extractions were completed. The objectives of this project were to propose a degradation scheme for the test toxin in the MOF-199 pores based on the data from these three experimental techniques.

The objectives of the last project focus on the production of a POM-MOF structure on cotton. The first objective was to develop a method to grow the POM-MOF on the surface of the cotton at room temperature. Next, these materials were characterized to evaluate moisture content, crystal structure, and metal content to prove that a POM-MOF-cotton specimen had indeed been created. Then, the final objective was to determine if the specimen containing the MOF encapsulated POM particles and attached to cotton removed more test toxin than the control fabric specimens. Ideally, confirming that encapsulation of the POM in the MOF on the cotton is a beneficial combination of adsorption properties and self-decontamination

properties while maintaining the thermal comfort of the original cotton material.

1.4. REFERENCES

(1) (September 11, 2013). Pesticide Illness & Injury Surveillance. *National Institute for Occupational Safety and Health*. Retreived September 12, 2013, from http://www.cdc.gov/niosh/topics/pesticides/.

(2) Britt, D.; Furukawa, H.; Wang, B.; Glover, T. G.; Yaghi, O. M. *P. Natl. Acad. Sci. USA* **2009**, 106 (49), 20637-20640.

(3) Britt, D.; Tranchemontagne, D.; Yaghi, O.M. *P. Natl. Acad. Sci. USA* **2009**, 105 (33), 11623-11627.

(4) Furukawa, H.; Yaghi, O. M. *J. Am. Chem. Soc.* **2009**, 131, 8875-8883.

(5) Schlichte, K.; Kratzke, T.; Kaskel, S. *Microporous Mesoporous Mater.*, **2004**, 73, 81–88.

(6) Song, J.; Luo, Z.; Furakawa, H.; Yaghi, O. M.; Hardcastle, K. I.; Hill, C. L. *J. Am. Chem. Soc.* **2011,** 133, 16839-16846.

(7) Guo, W.; Luo, Z.; Song, J.; Zhu, G.; Zhao, C.; Lv, H.; Vickers, J. W.; Geletii, Y. V.; Djamaladdin, G. M.; Hill, C. L. (2012) Multi-electron Transfer Catalysts for Air-Based Organic Oxidations and Water Oxidation. In *Complexity in Chemistry and Beyond: Interplay Theory and Experiment.* (pp. 229-242) NATO Science for Peace and Security Series B: Physics and Biophysics.

(8) Hill, C. L.; Prosser-McCartha, C. M. *Coord Chem Rev* **1995**, 143, 407.

(9) Neumann, R. *Prog Inorg Chem* **1998,** 47, 317.

(10) Mizuno, N.; Misono, M. *Chem Rev* **1998,** 98, 199.

(11) Okuhara, T.; Mizuno, N.; Misono, M. *Appl Catal A* **2001,** 222, 63.

(12) Nakagawa, Y.; Kamata, K.; Kotani, M.; Yamaguchi, K.; Mizuno, N. *Angew Chem Int Ed* **2005,** 44, 5136.

(13) Juan-Alcañiz, J.; Gascon, J.; Kapteijn, F. *J Mater Chem* **2012**, 22, 10102.

(14) Maksimchuk, N.V.; Timofeeva, M. N.; Melgunov, M. S.; Shmakov, A. N.; Chesalov, Y. A.; Dybtsev, D. N.; Fedin, V. P.; Kholdeeva, O. A. *J Catal* **2008,** 257, 315.

(15) Maksimchuk, N. V.; Kovalenko, K. A.; Arzumanov, S. S.; Chesalov, Y. A.; Melgunov, M. S.; Stepanov, A. G.; Fedin, V. P.; Kholdeeva, O. A. *Inorg Chem* **2010,** 49, 2920.

(16) Juan-Alcañiz, J.; Ramos-Fernandez, E. V.; Lafont, U.; Gascon, J.; Kapteijn, F. *J Catal* **2010,** 269, 229.

(17) Juan-Alcañiz, J.; Goesten, M.; Martinez-Joaristi, A.; Stavitski, E.; Petukhov, A. V.; Gascon, J.; Kapteijn, F. *Chem Commun* **2011,** 47, 8578.

(18) Kim, J.; Yun, S.; Ounaies, Z. *Macromolecules* **2006,** 39, 4202–4206.

(19) Wang, Z.; Hauser, P. J.; Laine, J.; Rojas, O. J. *J. Adhes. Sci. Technol.* **2011,** 25, 643-660.

(20) da Silva Pinto, M.; Sierra-Avila, C. A.; Hinestroza, J. P. *Cellulose.* **2012,** 19, 1771-1779.

(21) Tranchemontagne, D. J.; Hunt, J. R.; Yaghi, O. M. *Tetrahedron* **2008,** 64, 8553-8557.

(22) Schlesinger, M.; Schulze, S.; Hietschold, M.; Mehring, M. *Microporous Mesoporous Mater.* **2010,** 132, 121-127.

(23) Levin HS, Rodnitzky RL (1976) *Behavioral Effects of Organophosphate Pesticides in Man.* Clinical Toxicology 9(3): 391-405.

(24) Tafuri J, Roberts J (1987) *Organophosphate Poisoning*. Annals of Emergency Medicine 16: 193-202.

(25) Garcia SJ, Abu-Qare AW, Meeker-O'Connell WA, Borton AJ, Abou-Donia MB (2003) *Methyl Parathion: A Review of Health Effects*. Journal of Toxicology and Environmental Health, Part B 6: 185-210.

(26) Morgan DP, Hetzler HL, Slach EF, et al. (1977) *Urinary excretion of paranitrophenol and alkyl phosphates following ingestion of methyl or ethyl parathion by human subjects.* Archives of Environmental Contamination and Toxicology 6: 159-173.

(27) World Health Organization. WHO recommended classification of pesticides by hazard and guidelines to classification 2000-2002. WHO/PCS/01.5, 0ed, Geneva, 2002.

(28) Gianessi LP (1992) US Pesticide Use Trends: 1966-1989. Resources for the Future, Washington, DC.

(29) Abou-Donia MB (1994) Organophosphorus pesticides. In Handbook of Neurotoxicology, eds. Chang LW and Dyer RS, New York: Marcel Dekker, 419–473.

(30) O'Neil MJ, et al. (2006) The Merck index: an encyclopedia of chemicals, drugs, and biologicals. 14th ed. Whitehouse Station, NJ: Merck.

(31) Tomlin CDS (1997) The Pesticide Manual, 11th ed. British Crop Protection Council, Surrey, UK.

(32) Keith LH, Walters DB, ed. (1985) Compendium of safety data sheets for research and industrial chemicals. Parts I, II, and III. Deerfield Beach, FL: VCH Publishers, 1136.

(33) Sunshine I (1969) CRC Handbook of analytical toxicology. Cleveland, OH: The Chemical Rubber Co., 522.

(34) Sanders PF, Seiber JN (1983) *A chamber for measuring volatilization of pesticides from model soil and water disposal systems*. Chemosphere 12 (7/8): 999-1012.

(35) Senthilnathan J, Philip L (2009) *Removal of mixed pesticides from drinking water system by photodegradation using suspended and immobilized* TiO_2. Journal of Environmental Science and Health Part B 44: 262-270.

(36) World Health Organization (1993) *Enviromental Health Criteria 145, Methyl Parathion*. http://www.inchem.org/documents/ehc/ehc/ehc145.htm

(37) Adhya TK, Wahid PA, Sethunathan N (1987) *Persistence and biodegradation of selected organophosphorus insecticides in flooded versus non-flooded soils*. Biology and Fertility of Soils 4: 36-40.

(38) Brahmaprakash GP, Panda S, Sethunathan N (1987) *Relative persistence of hexachlorocyclohexane, methyl parathion and carbofuran in an alluvial soil under flooded and non-flooded conditions*. Agriculture, Ecosystems & Environment 19: 29-39.

(39) Baker RD, Applegate HG (1970) *Effect of temperature and ultraviolet radiation on the persistence of methyl parathion and DDT in soils*. Journal of Agronomy and Crop Science 62: 509-512.

(40) Ou L, Rao PS, Davidson JM. (1983) *Methyl parathion degradation in soil: Influence of soil-water tension*. Soil Biology & Biochemistry 15: 211-215.

(41) Sharmila M, Ramanand K, Adhya TK, et al. (1988) *Temperature and the persistence of methyl parathion in a flooded soil*. Soil Biology & Biochemistry 20: 399-401.

(42) McLean JE, Sims RC, Doucette WJ, et al. (1988) *Evaluation of mobility of pesticides in soil using U.S. EPA Methodology*. Journal of Environmental Engineering 114: 689-703.

(43) Gerstl Z, Helling CS (1985) *Fate of bound methyl parathion residues in soils as affected by agronomic practices*. Soil Biology & Biochemistry 17:667-673.

(44) Hansch, C., Leo, A., D. Hoekman (1995) Exploring QSAR - Hydrophobic, Electronic, and Steric Constants. Washington, DC: American Chemical Society, 44.

(45) Hong Z, Rockhold RW, Baker RC, Kramer RE, Ho IK (2001) *Effects of single or reapeated dermal exposure to methyl parathion on behavior and blood cholinesterase activity in rats*. Journal of Biomedical Science 8: 467-474.

(46) Isbister GK, Mills K, Friberg LE, Hodge M, O'Connor E, Patel R, Abeyewardene M, Eddleston M (2007) *Human methyl parathion poisoning*. Clinical Toxicology 45: 956-960.

(47) Dzyadevych SV, Sodatkin AP, Chovelon J-M (2002) *Assessment of the toxicity of methyl parathion and its photodegradation products in water samples using conductometric enzyme biosensors*. Analytica Chimica Acta 459: 33-41.

CHAPTER 2

CuBTC METAL-ORGANIC FRAMEWORKS ENMESHED IN POLYACRYLONITRILE FIBROUS MEMBRANE REMOVE METHYL PARATHION FROM SOLUTIONS

2.1. Abstract

A method is presented to immobilize Cu-BTC metal-organic framework (MOF-199) particles by enmeshing them in nonwoven polyacrylonitrile (PAN) nanofibers creating a fibrous membrane with the potential ability to remove chemical warfare agents or pesticides from solution. These membranes were shown to effectively adsorb methyl parathion, an organophosphate pesticide. Based on solubility theory and experimental results, partitioning was determined to be the main mechanism of removal. After 2 hours, the PAN/MOF-199 membranes removed 88% more methyl parathion than the unmodified PAN membranes and 62% as much as the MOF-199 crystal powder. Since the MOF particles were enmeshed in the PAN fiber mats, the MOF particles were in a workable and flexible substrate. Potential applications of these functionalized fibrous membranes include protective clothing for agricultural workers or military personnel as well as filtration media.

2.2. Introduction

Organophosphates (OPs) are a group of organic phosphorous compounds that are of wide interest due to their use as neurotoxic pesticides/insecticides. OPs pose a threat to humans through dermal absorption as they can bind to acetylcholinesterase, thereby potentially disrupting nervous impulses and inhibiting the functions of nerve cells[1]. Exploring novel and efficient ways to isolate or decontaminate OPs, with

minimal environmental impact, has become a global necessity[2]. Numerous ways to degrade OPs have been reported to date, including enzymatic biodegradation[3], electrochemical[4], catalytic oxidation[5], atmospheric pressure plasma[6], photolytic[7], and destructive adsorption[8] methods. Hydrolysis of OPs through cleavage of the P-S bond using solid hosts has been widely implemented using TiO_2[9], MgO[8,10], nanometer-sized Al_2O_3[11,12], ZnO[13], Au/TiO_2[14], activated carbons[15], polymers[16], and mesoporous silica[17]. There also has been interest in the adsorption and hydrolysis of OPs in clay[18, 19], soil components[20], and zeolites[21, 22].

Immobilization of any of the previously mentioned adsorbents and active compounds on nonwoven substrates can result in novel and promising materials for protective clothing. The advantages of using nonwoven substrates include increased breathability, decreased weight, and higher levels of comfort. Nonwovens can be produced using several methods such as meltblowing, spunbonding, as well as electrospinning. Nanofibrous structures, commonly produced with electrospinning, are beneficial due to their small fiber diameter, large surface areas that lead to a high surface-to-volume ratio, and small interfiber pore sizes in the membrane[23].

Several active agents have been incorporated into nonwoven nanofibrous mats creating materials with the ability to bind or detoxify chemical warfare agents and pesticides. One example of this has been the surface modification of nanofibers by creating reactive groups such as oximes, cyclodextrins and chloramines[24]. Functionalized polymers synthesized from β- cyclodextrin and o-iodosobenzoic acid and processed into fibrous membranes have also shown decontamination of nerve agents through hydrolysis[25]. Metal and metal oxide nanoparticles (Ag, MgO, Ni, Ti,

etc.), which have proven abilities to decompose warfare agents, have also been embedded in the nanofibers[8]. However, a major challenge with these technologies lies with the fact that in some cases the degradation products of OPs result in even more toxic substances.

Creating a fabric that can keep the wearer safe, while maintaining a breathable and lightweight fabric, has become an important challenge and metal organic frameworks (MOFs) have potential to meet this challenge. MOFs are crystalline nanoporous materials that consist of metal clusters held together by multifunctional organic linkers[26-28]. MOFs are of interest due to their large surface area and their controllable pore size leading to an increased potential for selectively adsorbing chemicals and gases[29-35].

We hereby report on a method to immobilize copper(II)-benzene-1,3,5-tricarboxylate (Cu-BTC or MOF-199) particles by enmeshing them with nonwoven polyacrylonitrile (PAN) nanofibers and the ability of these membranes to absorb methyl parathion, a pesticide commonly used as a simulant for VX warfare agent.

2.3. Experimental

2.3.1. Fiber Formation

Polyacrylonitrile (PAN) was purchased from Sigma Aldrich (St. Louis, MO) and used as received. PAN solutions were made using reagent grade dimethylformamide (DMF) from Mallinckrodt Chemicals (Phillipsburg, NJ). A 14% wt PAN solution concentration was selected after completing several preliminary experiments exploring the desired viscosity for the electrospinning process. A flow rate of 50 μL/h was used with an applied voltage of 20 kV, and a grounded metal

screen covered with aluminum foil, placed at a distance of 20 cm from the syringe tip, was used as the counter electrode.

Commercially available MOF-199, Basolite C-300 (BASF, Florham Park, NJ), with a reported average particle size of about 16 μm, 1500-2100 m^2/g BET surface area, 200 °C reactivation temperature, and 0.35 g/cm^3 bulk density was used. In a typical synthesis, after complete dissolution of the polymer, MOF-199 particles were added to a weight ratio PAN/MOF-199 of 7:3. The PAN/MOF mixture was stirred for 3 h and electrospun. The resulting fibers were reactivated by heating them to 150 °C for 1 h.

2.3.2. Nonwoven Fiber Mat Characterization

Scanning electron microscopy (SEM) was conducted using a LEO 1550 FE-SEM from Carl Zeiss, Inc. (Thornwood, NY) and a Leica 440 SEM (Wetzlar, Germany). Image analysis was performed using ImageJ (National Institutes of Health, Bethesda, MD). Thermogravimetric analysis (TGA) was completed using a TGA Q500 from TA Instruments (New Castle, DE) ramping from 30 °C to 1000 °C at 10 °C/min and keeping isothermal at 1000 °C for 15 min. A Nicolet Magna IR 560 spectrometer FTIR (Thermo Fisher Scientific Inc., Waltham, MA) with a MIRacle Attenuated Total Reflectance (ATR) attachment (PIKE Technologies, Madison, WI) was used to obtain all spectra with 130 scans and a resolution of 2 cm^{-1}. Porous Materials, Inc. (Ithaca, NY) used Krypton gas as an adsorbate on a PMI BET Sorptometer 201A to collect the BET surface area data for Figure 3. Furukawa Hiroyasu and Omar Yaghi provided Nitrogen BET adsorption isotherms obtained on a Autosorb-1 (Quantachrome Instruments, Boynton Beach, FL) shown in Figure 4.

2.3.3. Adsorption Performance Experiments with HPLC

PAN/MOF-199 fiber specimens were weighed to 0.1 g. MOF particles specimens weighed 0.02 g and PAN fiber specimens weighed 0.08 g. Each specimen was immersed in a vial containing 10 mL of HPLC grade hexane (EMD Millipore Chemicals, Billerica, MA) with 250 μg of methyl parathion for 5, 15, 30, 45, or 120 minutes. After each designated experimental time, a 1.5-mL aliquot was removed from the vial using a 5-mL syringe with Luer-Lok Tips (BD Biosciences, Franklin Lakes, NJ) and filtered using a Titan2® nylon 0.20-μm pore sized syringe filter (SUN-Sri, Rockwood, TN). Each aliquot was then transferred to a vial for high performance liquid chromatography (HPLC) analysis.

A reverse phase HPLC combined with a diode array UV-vis detector (DAD) from Agilent (Santa Clara, CA) HP series 1200 was used to measure the concentrations of methyl parathion. The injection volume was 20 μL. An Agilent XDB-C18 reversed phase column with 5-μm particle size, 4.6 x 150-mm dimension was used, at a temperature of 25 °C. The mobile phase consisted of 50:50 volume ratio of acetonitrile and water with 0.5 v % formic acid, and the run time was 22 min. The UV-vis detector was set to scan at 280 and 320 nm and a single-quadrupole Agilent 6130 was used.

Standards and calibration curves for methyl parathion and its degradation products were used to adjust for any instrument drift of the HPLC-DAD. Methyl parathion (PS-94), OOO-trimethyl phosphoric thiourate (F2570), and 4-nitrophenol (O-896) were purchased from Chem Service Incorporated (West Chester, PA). The retention time observed for methyl parathion was 13.4 min. No degradation products

were observed in the specimens based on the lack of any peaks other than those corresponding to methyl parathion. Quantification of methyl parathion was performed using data from the DAD detector.

2.3.4. Statistical Analysis

Each experiment was performed using three replicates. Two-way analyses of variance (ANOVA) followed by a post hoc mean comparisons with Tukey correction were completed using JMP 9 (SAS, Cary, NC). The statistical tests were run to determine if significant differences were evident between the amounts of methyl parathion detected based on two nominal variables: reaction time (5, 15, 30, 45, 120 min) and specimen type (MOF, PAN, PAN/MOF-199, and methyl parathion standard).

2.4. Results and Discussion

2.4.1. Fibrous Membrane Morphology

The morphology of the MOF particles and the submicron fiber structure in which they were enmeshed are of equal importance to the functionality of the composite. Figure 2.1a is a low magnification SEM image of the PAN/MOF-199 composite fibers showing how the MOF-199 particles were enmeshed throughout the fiber mat. The high magnification SEM image in Figure 2.1b shows pitted MOF-199 particles surrounded by the PAN nanofibers. We believe that the pitted surface morphology of MOF-199 particles, observed in Figure 2.1b, was due to exposure to DMF. To confirm this observation, Figure 2.2 shows MOF-199 particles that have been exposed to DMF for 0 h, 3 h, and 6 h. Pristine MOF-199 particles (Figure 2.2a) exhibit very defined edges with little to no surface pitting. After 3 h of DMF exposure

(Figure 2.2b), the edges of the MOF-199 particles appear more rounded. Surface pitting was clearly present, and smaller pieces of broken up MOF-199 particles were observed on the surface of the larger particles. The MOF-199 particles exposed to DMF for 6 h (Figure 2.2c) displayed similar morphological features but to a greater extent than those exposed to DMF for 3h.

Based on both Figures 2.1a and 2.1b, the average PAN fiber diameter was determined to be 102 nm with a standard deviation of 47 nm. Image analysis also showed that the average MOF-199 particle size was 7.5 μm with a standard deviation of 6.3 μm. This average is smaller than the measured value of the as received Basolite C300, which was 12.6 μm with a standard deviation of 8.0 μm. The differences in particle size could be explained by how the particles interact with the PAN/DMF solution during the electrospinning process. The 3 h of mixing used to ensure good uniformity of the solution could have broken up large particle aggregates of which we see evidence in Figure 2.2b. It is also possible that larger and therefore heavier particles settled out of solution during the long period used to electrospin the membranes.

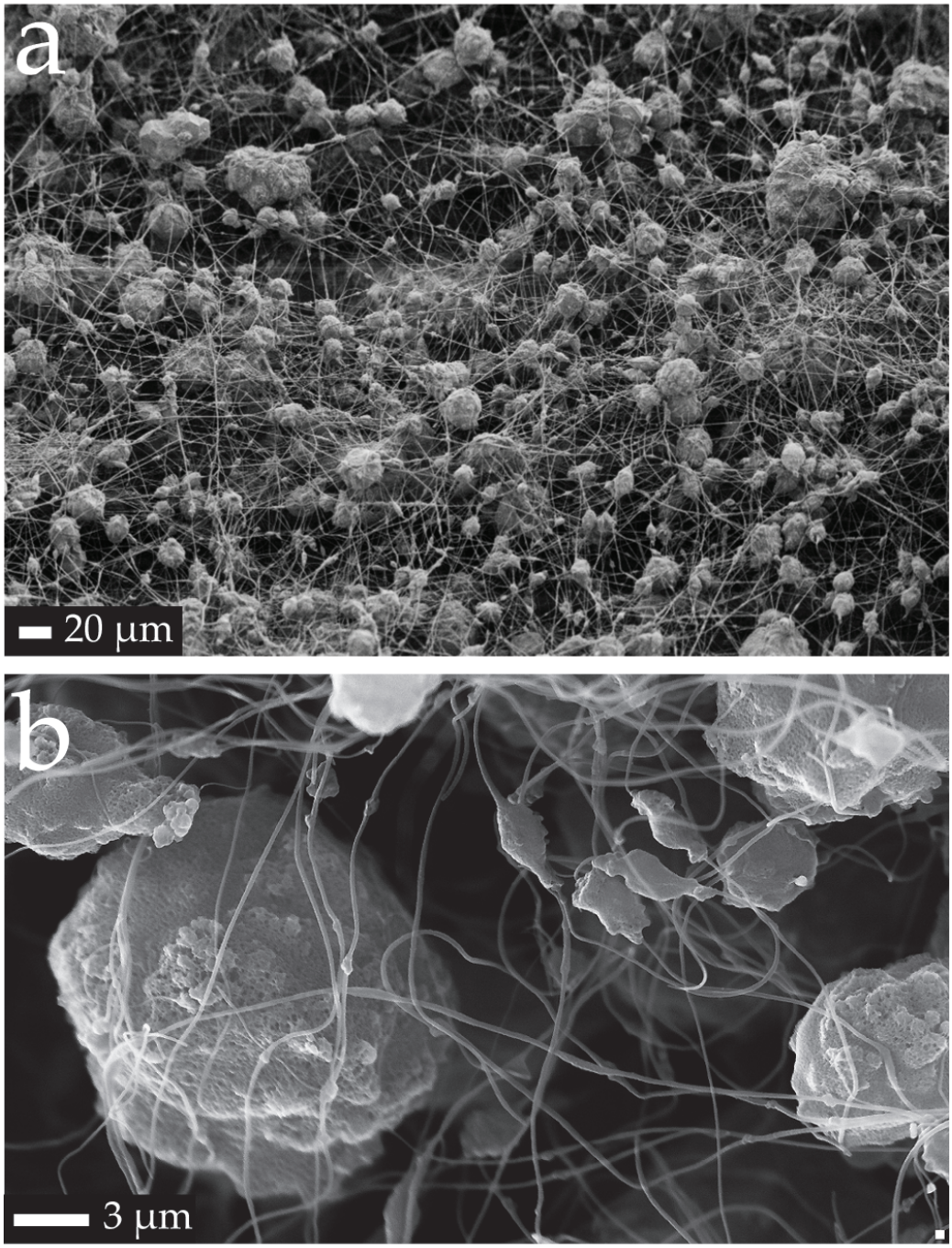

Figure 2.1. SEM images of two PAN/ MOF-199 fibrous membranes at (a) low magnification and (b) high magnification. The low magnification shows how the MOF-199 particles are enmeshed throughout the fiber mat, while the high magnification shows surface pitted MOF-199 particles surrounded by the PAN nanofibers.

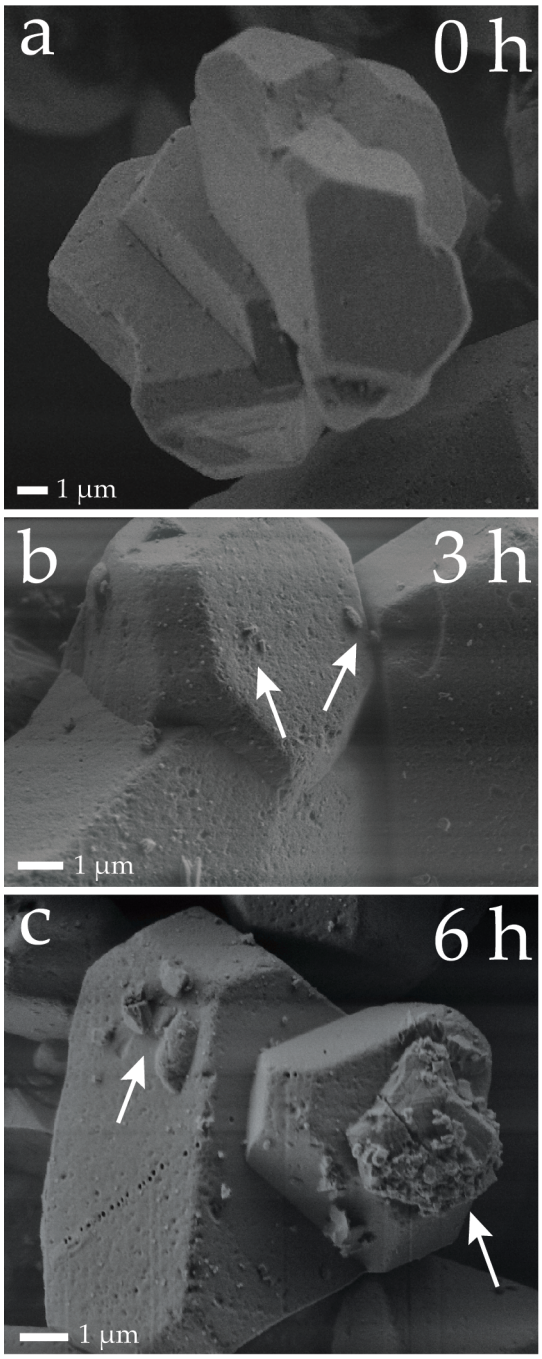

Figure 2.2. SEM images of MOF-199 particles that were (a) untreated, (b) mixed with DMF for 3 h and (c) mixed with DMF for 6 h. Arrows indicate broken up and deposited pieces of MOF-199 that result from introduction of DMF and mixing.

2.4.2. BET Surface Area Measurements

BET surface area analyses are shown in Figure 2.3. As expected, the Basolite MOF-199 particles exhibited the highest surface area, about an order of magnitude higher than that of the PAN/MOF-199 membrane. The PAN/MOF-199 membrane had nearly two orders of magnitudes more surface area than the PAN fibers. For the PAN/MOF-199 membrane, the values in Figure 2.3 theoretically correspond to a PAN/MOF content ratio of 87/13 based on surface area assumptions of a circular fiber, which is in quantitative agreement with the predicted ratio of 80/20.

Adsorption isotherms for the PAN/MOF-199 and the PAN fibrous membranes are presented in Figure 2.4. The specific BET surface area calculated from these isotherms was approximately 220 m^2/g for the PAN/MOF-199 and 4 m^2/g for the PAN fibrous membranes. These values for surface areas are within the same order of magnitude as the values reported in Figure 2.3. The adsorption isotherm for the PAN/MOF-199 fibrous membrane (Figure 2.4a) shows a Type I shape; this shape indicates a primarily microporous composite[35]. The characteristic plateau observed in a Type I shape indicates that little adsorption occurs after the micropores are filled[36]. In the literature, MOF-199 particles have also been reported to have Type I adsorption behavior[37]. It can be seen that incorporation of the MOF-199 particles significantly increases the surface area of the membrane compared to the PAN control specimen, but does not change the type of adsorption isotherm observed for the pristine MOF-199 particles.

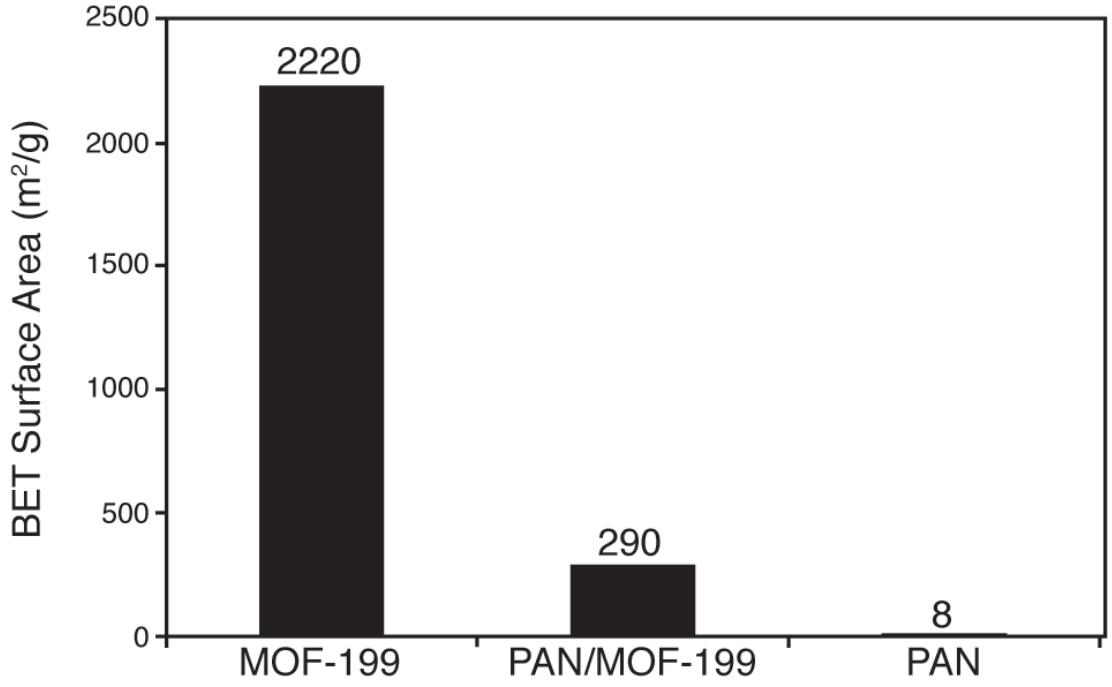

Figure 2.3. BET Surface area for MOF-199, PAN/MOF-199, and PAN.

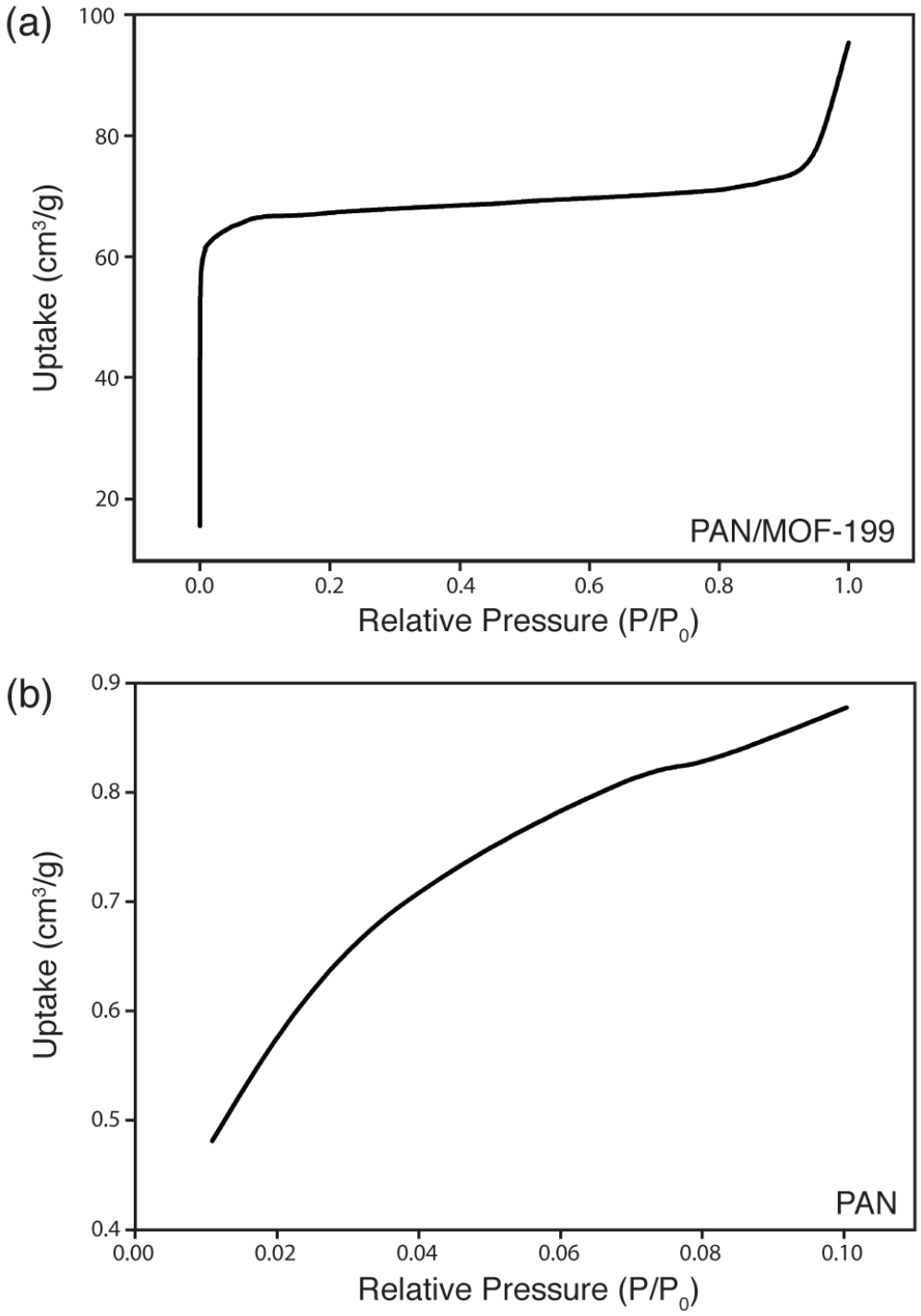

Figure 2.4. Adsorption isotherms of (a) PAN/MOF-199 and (b) PAN.

2.4.3. Thermal Analysis of PAN/MOF-199 Composite Fiber

The residual weight percent of the specimens after heating them to 1000 °C was 28.9 % for the MOF particles, 8.3 % for the PAN/MOF-199 fibrous membranes, and 0.37 % for the PAN control membrane. Assuming that the remaining material was predominately Cu, it can be determined that in the PAN/MOF-199 fibrous membrane had a 72/28 PAN/MOF-199 weight ratio.

The thermal stability of the membranes was studied in order to determine an appropriate temperature to reactivate the MOF-199 particles without destroying the PAN fibers in which they are enmeshed. PAN was reported to decompose between 230 °C - 340 °C[38] which is in agreement with our experiment as shown in Figure 2.5. The MOF-199 specimen had the greatest weight loss near 333 °C and the PAN/MOF-199 membranes exhibited significant weight loss around two temperatures: 314 °C and 327 °C. Since the PAN and MOF-199 samples lose weight at similar temperature ranges, overlapping degradation of both components was occurring simultaneously in the PAN/MOF-199 fibrous membrane. The onset temperature for the first major weight loss observed in the PAN/MOF-199 membrane was near 290 °C. The degradation of the MOF-199 contributed to weight loss around 330 °C. The thermogram indicates that the specimen absorbed water as shown from the large weight loss illustrated by the derivative weight loss versus temperature (Figure 2.5b) around 100 °C. The MOF particles adsorbed the highest percentage of water, followed by the PAN/MOF-199 fibrous membrane, while PAN adsorbed the least amount of water.

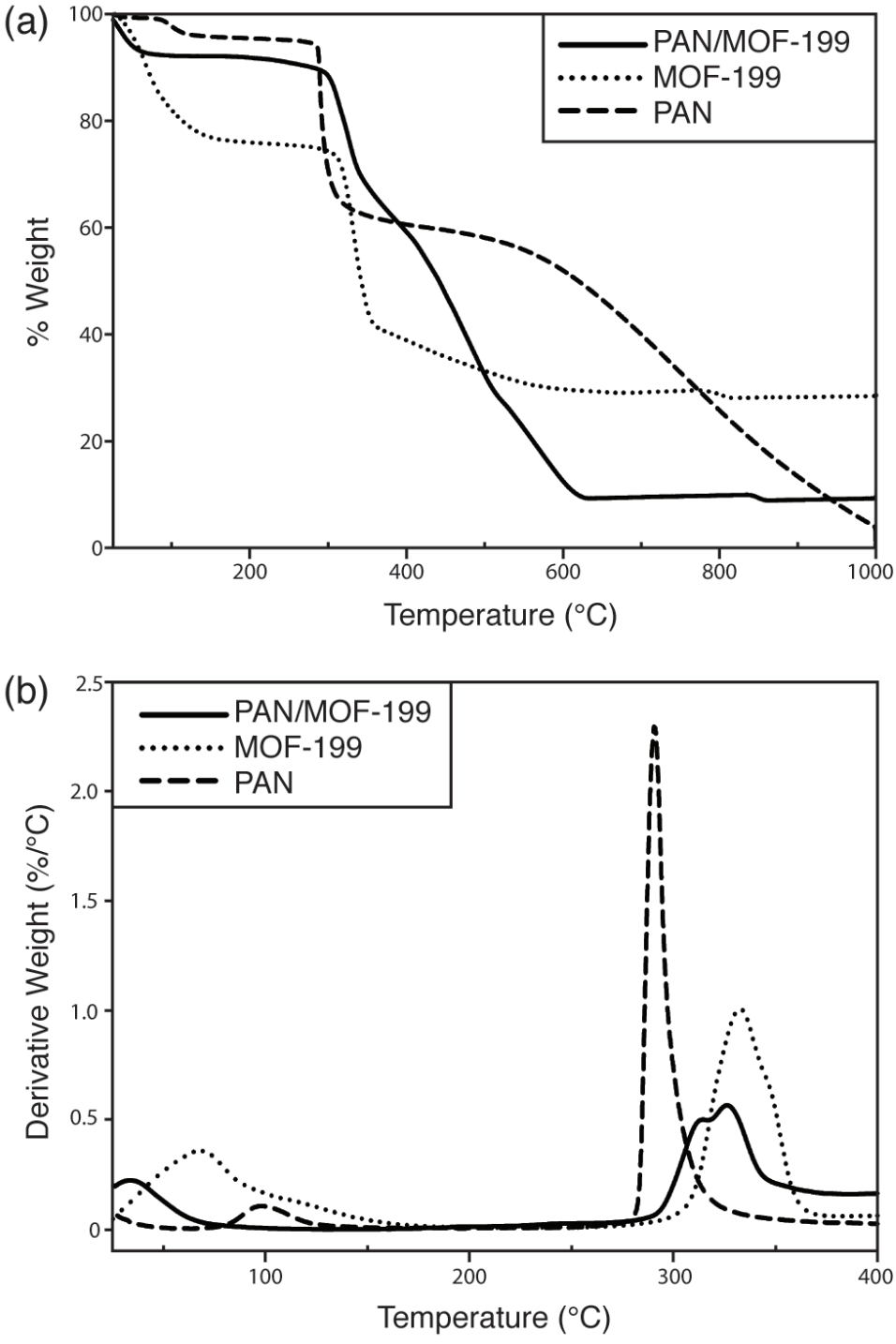

Figure 2.5. (a) TGA thermograph showing weight loss (%) for the three specimen types based on temperature (°C) and (b) derivative of TGA thermograph showing the change in percent weight loss per degree Celsius (%/°C) versus temperature (°C).

2.4.4. FTIR-ATR Analysis

Each specimen was characterized using IR before and after being exposed to methyl parathion. The IR spectrum (Figure 2.6) shows that methyl parathion could not be detected in any of the three specimens (MOF, PAN, and PAN/MOF-199) after exposure. No change or shift in the peaks for any of the three specimens was observed either. This observation leads us to believe that methyl parathion was partitioning into the MOF particles, and no binding reaction altering the functional groups of the MOF structure was observed. A past study has shown that partitioning based on physical entrapment, hydrophobic interaction, and dispersion forces occurred with aroma chemicals on a cotton fabric[39]. These types of interactions would not result in a change of functional groups observed in FTIR, and it appears that a similar mechanism is likely in this case. It should also be noted that despite not observing adsorbed agents on the MOF with FTIR-ATR, water extractions of the MOF showed that some methyl parathion and 4-nitrophenol were retained on the substrate.

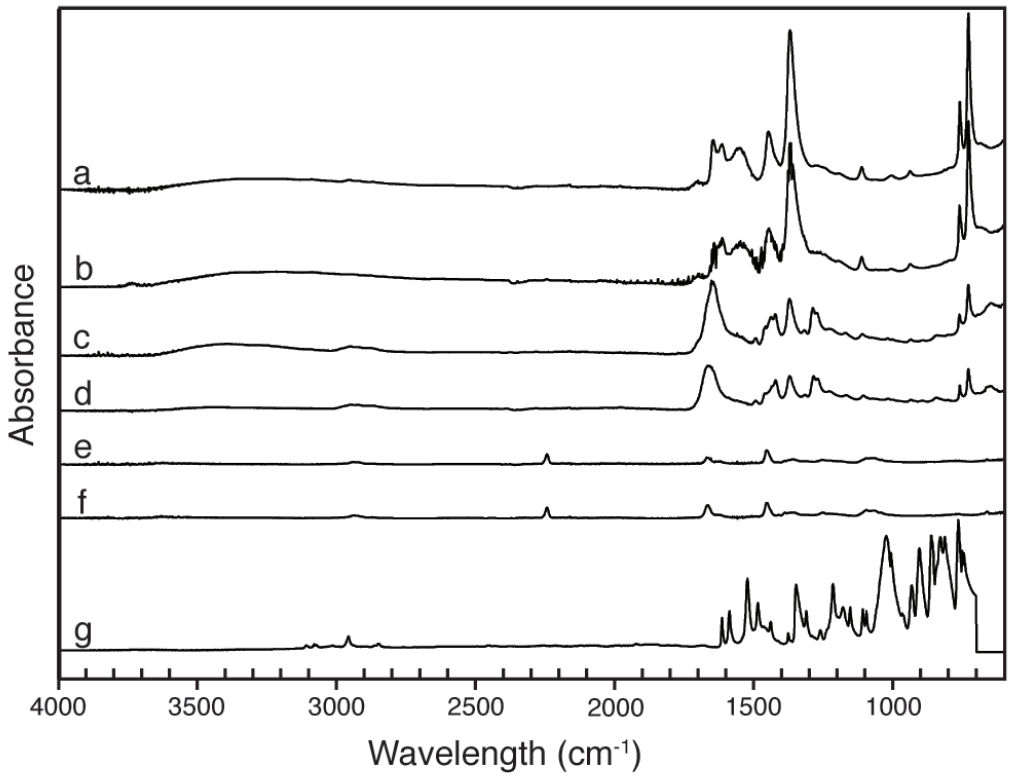

Figure 2.6. IR absorbance spectra of (a) MOF, (b) MOF treated with methyl parathion, (c) PAN/MOF-199, (d) PAN/MOF-199 treated with methyl parathion, (e) PAN, (f) PAN treated with methyl parathion, and (g) methyl parathion.

2.4.5. Methyl Parathion Removal

Removal of methyl parathion was measured via HPLC analysis by quantifying the decrease in the content of methyl parathion from a hexane solution. The experiments reported in this manuscript were performed in solution because it was much safer for an academic laboratory setup; however, it is noted that contamination with an aerosol would be closer to practical applications. The ANOVA analysis, Table 2.1, shows that reaction time, specimen type, and interaction between reaction time and specimen type had significant effects on the amount of methyl parathion removed from solution.

The *post hoc* mean comparison with Tukey correction at a 95% confidence interval ($\alpha = 0.05$, $Q = 3.68$) is presented in Table 2.2. The most interesting aspect of this analysis was that for each time point between 5 and 45 min the amount of methyl parathion removed by the PAN and PAN/MOF-199 samples were not significantly different from one another, but both were significantly different than the amount removed by MOF-199. However, after 120 min the PAN/MOF-199 and the MOF-199 specimens did not remove significantly different amounts of methyl parathion, but their removal results were significantly different from the one corresponding to PAN fibers. These results show that given enough time, the PAN/MOF-199 samples go from performing in a similar manner to the PAN fibers to performing more like the MOF-199 particles. Statistically, these results confirm that the interaction term between time and type of substrate plays a significant role in the amount of methyl parathion removed from solution. Specifically, within the time range between 5 and 120 min only the PAN/MOF-199 specimen exhibits differences over time because

Table 2.1. Statistical results from a two-way ANOVA comparing the amount of methyl parathion amounts in hexane based on reaction time and specimen type**.**

Effect	**F Ratio**	**Probability > F**	**Significant Effect?**
Complete ANOVA	93.5	< 0.0001	Yes
Reaction Time	8.5	0.0058	Yes
Specimen Type	225.2	<0.0001	Yes
Interaction between Reaction Time and Specimen Type	4.3	0.0201	Yes

Table 2.2. Results of the post hoc mean comparison with Tukey correction at a 95% confidence interval ($\alpha = 0.05$, $Q = 3.68$) of the removed amount of methyl parathion (μg) based on reaction time and specimen type. Numbers reported are least square mean with the lower and upper 95% confidence intervals in parenthesis. Arabic letters indicate which samples are significantly different across sample type for each time point. For example, at 120 minutes, the PAN/MOF-199 and MOF-199 are not significantly different but are both significantly different from the PAN. Greek letters indicate which samples are significantly different across time points for each sample type.

Time (min)	PAN	PAN/MOF-199	MOF-199
5	3.45 (-20.73, 27.63)$^{a\alpha}$	44.49 (20.31, 68.68)$^{a\alpha}$	164.91 (140.73, 189.09)$^{b\alpha}$
15	5.49 (-18.69, 29.67)$^{a\alpha}$	47.52 (23.34, 71.70)$^{a\alpha}$	142.96 (118.78, 167.14)$^{b\alpha}$
30	6.48 (-17.70, 30.67)$^{a\alpha}$	61.29 (37.11, 85.47)$^{a\alpha}$	163.04 (138.85, 187.22)$^{b\alpha}$
45	17.16 (-7.02, 41.34)$^{a\alpha}$	72.64 (48.46, 96.83)$^{a\alpha}$	146.88 (122.69, 171.06)$^{b\alpha}$
120	12.25 (-11.93, 36.43)$^{a\alpha}$	101.16 (76.98, 125.34)$^{b\alpha}$	161.93 (137.74, 186.11)$^{b\alpha}$

these samples approach their equilibrium methyl parathion removal within this time range.

With respect to time, MOF-199 particle specimens exhibited little variation in the amount of removed methyl parathion between 5 and 120 min (Table 2.2). A small amount of methyl parathion that did not vary significantly with time was retained on the control PAN membrane. Whereas, the PAN/MOF-199 fibrous membrane exhibited higher removal of methyl parathion and it increased with time. This difference is likely due to the time needed for diffusion of methyl parathion to the MOF-199 particles within the fibrous membrane. For each time point, more variation can also be observed for the PAN/MOF-199 samples. This variation in performance can be related to variability in how the MOF-199 is distributed in the fiber mats, so increasing the size of the sample could reduce this variability.

The removal of methyl parathion as a function of time was fit with a modified hyperbolic equation:

$$\Gamma = \frac{\Gamma_{\max} K t}{1 + K t} \tag{2.1}$$

where Γ is the amount of methyl parathion removed in μg, Γ_{max} is the maximum amount of methyl parathion removed by each sample (Table 2.3), K is an equilibrium constant (Table 2.3), and t is time in min. This equation is similar to the Langmuir adsorption equation. It was observed that removal with the MOF particles reaches equilibrium very quickly (Table 2.2) which was reflected in the model (Table 2.3). The PAN/MOF-199 membranes appear to be approaching the equilibrium removal of

methyl parathion shortly after 120 min. At about 120 min, the model indicates that the PAN/MOF-199 membrane would remove 90% of the available methyl parathion. The PAN specimens approach equilibrium after a much longer period of time than the MOF or the PAN/MOF-199. By incorporating the MOF-199 particles into the PAN fiber mats, it is clear that the limiting factor for removal is the diffusion time for the methyl parathion to reach all of the MOF particles.

Table 2.3. Best fit parameters for non-linear regression for MOF-199, PAN/MOF-199, and PAN based on Equation 2.1. Evaluation of Equation 2.1 for the time in min to 90% of Γ_{max} is also listed.

Specimen	Γ_{max}, Equilibrium amount of methyl parathion removed (μg)	*K*, Equation constant (min^{-1})	Time to 90% of Γ_{max} (min)
MOF-199	155.9	8.56×10^{6}	1.05×10^{-6}
PAN/MOF-199	102.4	7.18×10^{-2}	1.25×10^{2}
PAN	16.89	4.10×10^{-2}	2.20×10^{2}

2.4.6. Proposed Mechanism of Methyl Parathion Removal from Solution

We propose that the mechanism for removal of methyl parathion from the hexane solution was likely due to partitioning of the methyl parathion into the MOF-199 structure. The IR analysis of the MOF-199 structure before and after methyl parathion exposure showed no indication of chemical change to the MOF structure. It is probable that initial removal of methyl parathion was driven by relative solubility. Thus, solubility parameter calculations were performed [40]. Table 2.4 shows the Hansen solubility parameters for MOF-199, methyl parathion, and hexane. The approximate Hansen solubility parameters for methyl parathion were estimated using Equations 2.2, 2.3 and 2.4 for the dispersion parameter (δ_d), polar parameter (δ_p), and the hydrogen-bonding parameter (δ_h)[40].

$$\delta_{\mathrm{d}} = \frac{\sum_z {}^z F_{\mathrm{d}}}{V} \tag{2.2}$$

$$\delta_{\mathrm{p}} = \frac{\left(\sum_z {}^z F_{\mathrm{p}}^2\right)^{\frac{1}{2}}}{V} * 0.5 \tag{2.3}$$

$$\delta_{\mathrm{h}} = \left(-\sum_z {}^z U_{\mathrm{h}}/V\right)^{1/2} \tag{2.4}$$

Values for F_d, F_p and U_h correspond to the dispersion group molar attraction contributions, polar group molar attraction contributions, and hydrogen bonding parameter group contributions, which are all based on each group in the chemical

structure of methyl parathion[40,41]. V represents the molar volume of methyl parathion in cm^3/mol.

The interaction radius for methyl parathion with hexane was calculated to be 11.96 $MPa^{1/2}$ with Equation 2.5[40]. This means that if the distance between two compounds in the 3D space defined by δ_d, δ_p, δ_h, is less than 11.96 $MPa^{1/2}$ it is likely that the two molecules will dissolve or be attracted to one another[40]. A distance of 6.34 $MPa^{1/2}$ separates methyl parathion and MOF-199, while a distance of 9.63 $MPa^{1/2}$ separates methyl parathion and hexane. This means that methyl parathion is likely to partition into the MOF-199 environment as opposed to hexane, explaining the removal of methyl parathion from the hexane solution.

$$ {}^{ij}R = [4({}^{i}\delta_{\mathrm{d}} - {}^{j}\delta_{\mathrm{d}})^2 + ({}^{i}\delta_{\mathrm{p}} - {}^{j}\delta_{\mathrm{p}})^2 + ({}^{i}\delta_{\mathrm{h}} - {}^{j}\delta_{\mathrm{h}})^2]^{1/2} \qquad (2.5) $$

Table 2.4. Hansen solubility parameters describing dispersion, polarity, and hydrogen-bonding properties of MOF-199, methyl parathion, and hexane.

Material	δ_d, $MPa^{1/2}$	δ_p, $MPa^{1/2}$	δ_h, $MPa^{1/2}$	Source
MOF-199	17.9	9.9	10.7	[42]
Methyl Parathion	19.0	4.6	7.4	Calculated [40, 41]
Hexane	14.9	0.0	0.0	[43]

2.5. Conclusion

MOF-199 was determined to be effective in removing methyl parathion from a solvent due to partitioning. The PAN/MOF-199 membranes can remove a target toxin in two hours 62% as effectively as the unmodified MOF-199 particles. By immobilizing MOF-199 in a fiber mat, a fibrous membrane was created that had the ability to remove 88% more toxin than the PAN control. There are a variety of potential applications for this workable substrate including protective clothing or its possible use as a controlled release matrix. It is possible that the method used in this research could be used to create fiber mats that contain pesticides. These pesticide impregnated fiber mats could be used as a functional textile with a slow release system, which could potentially serve as insecticide-treated mosquito nets. However, this would require further testing with a pesticide that exhibits lower human toxicity than methyl parathion.

2.6. Acknowledgements

Special thanks go to the other co-authors of the published version of this chapter, Fredrick O. Ochanda, Juan P. Hinestroza, and S. Kay Obenforf. Fredrick O. Ochanda made the fiber mats developed for this research project. This research was funded through grants from the Cornell Agricultural Experiment Station, North Central Regional Research Project NC 170 federal formula funds, Project NYC329801 received from Cooperative State Research, Education, and Extension Service, U.S. Department of Agriculture; College of Human Ecology; American Association of Textile Chemists and Colorists; and the Defense Threat Reduction Agency through the Department of Defense (Subaward No. 8980 G KB786). This work made use of the

Cornell Center for Materials Research Facilities supported by the National Science Foundation under Award Number DMR-0520404.

2.7. REFERENCES

(1) Banks, K. E.; Hunter, D. H.; Wachal, D. J. *Environ. Int.* **2005**, 31, 351–356.

(2) Yang, Y. C.; Baker, J. A.; Ward, J. R. *Chem. Rev.* **1992**, 92, 1729–1743.

(3) Wilcox, D. E. *Chem. Rev.* **1996**, 96, 2435–2458.

(4) Vlyssides, A.; Barampouti, E. M.; Mai, S.; Arapoglou, D.; Kotronarou, A. *Environ. Sci. Technol.* **2004**, 38, 6125–6131.

(5) Kolinko, P. A.; Kozlov, D. V. *Environ. Sci. Technol.* **2008**, 42, 4350–4355.

(6) Kim, D. B.; Gweon, B.; Moon, S. Y.; Choe, W. *Curr. Appl. Phys.* **2009**, 9, 1093–1096.

(7) Zuo, G. M.; Cheng, Z. X.; Li, G. W.; Shi, W. P.; Miao, T. *Chem. Eng. J.* **2007**, 128, 135–140.

(8) Lange, L. E.; Obendorf, S. K. *Arch. Environ. Con. Tox.* **2012,** 62(2), 185-194.

(9) Dai, K.; Peng, T. Y.; Chen, H.; Liu, J.; Zan, L. *Environ. Sci. Technol.* **2009**, 43, 1540–1545.

(10) Wagner, G. W.; Bartram, P. W.; Koper, O; Klabunde, K. J. *J. Phys. Chem. B* **1999**, 103, 3225–3228.

(11) Wagner, G. W.; Procell, L. R.; O'Connor, R. J.; Munavalli, S.; Carnes, C. L.; Kapoor, P. N.; Klabunde, K. J. *J. Am. Chem. Soc.* **2001**, 123, 1636–1644.

(12) Wagner, G. W.; Procell, L. R.; Munavalli, S. *J. Phys. Chem. C* **2007**, 111, 17564–17569.

(13) Mahato, T.H.; Prasad, G.K.; Singh, B.; Acharya, J.; Srivastava, A.R.; Vijayaraghavan, R. *J. Hazard. Mater.* **2009**, 165, 928–932.

(14) Panayotov, D. A.; Morris, J. R. *J. Phys. Chem. C* **2008**, 112, 7496–7502.

(15) Columbus, I.; Waysbort, D.; Shmueli, L.; Nir, I.; Kaplan, D. *Environ. Sci. Technol.* **2006**, 40, 3952–3958.

(16) Bromberg, L.; Schreuder-Gibson, H.; Creasy, W. R.; McGarvey, D. J.; Fry, R. A.; Hatton, T. A. *Ind. Eng. Chem. Res.* **2009**, 48, 1650–1659.

(17) Gomes, D. E. B.; Lins, R. D.; Pascutti, P. G.; Lei, C. H.; Soares, T. A. *J. Phys. Chem. B* **2010**, 114, 531–540.

(18) Seger, M. R.; Maciel, G. E. *Environ. Sci. Technol.* **2006**, 40, 797–802.

(19) Seger, M. R.; Maciel, G. E. *Environ. Sci. Technol.* **2006,** 40, 552-558.

(20) Seger, M. R.; Maciel, G. E. *Environ. Sci. Technol.* **2006**, 40, 791–796.

(21) Fei, X; Sun, G. *Ind. Eng. Chem. Res.* **2009**, 48, 5604–5609.

(22) Knagge, K.; Johnson, M.; Grassian, V. H.; Larsen, S. C. *Langmuir* **2006**, 22, 11077–11084.

(23) Srinivasan, G.; Reneker, D. H. *Polym. Int*. **1995,** 36, 195-201.

(24) Ramakrishna, S.; Fujihara, K.; Teo, W. E.; Yong, T.; Ma, Z.; Ramaseshan, R. *Mater. Today* **2006**, 9, 40-50.

(25) Ramaseshan, R.; Sundarrajan, S.; Liu, Y.; Barhate, R. S.; Lala N. L.; Ramakrishna, S. *Nanotechnology* **2006**, 17, 2947-2953.

(26) Eddaoudi, M.; Kim, J.; Rosi, N.; Vodak, D.; Wachter, J.; O'Keeffe, M.; Yaghi, O. M. *Science* **2002**, 295, 469–472.

(27) Bordiga, S.; Regli, L.; Bonino, F.; Groppo, E.; Lamberti, C.; Xiao, B.; Wheatley, P. S.; Morris, R. E.; Zecchina, A. *Phys. Chem. Chem. Phys.* **2007**, 9, 2676-2685.

(28) Prestipino, C.; Regli, L.; Vitillo, J. G.; Bonino, F.; Damin, A.;

Lamberti, C.; Zecchina, A.; Solari, P. L.; Kongshaug, K. O.; Bordiga, S. *Chem. Mater.* **2006**, 18, 1337-1346.

(29) Britt, D.; Furukawa, H.; Wang, B.; Glover, T. G.; Yaghi, O. M. *P. Natl. Acad. Sci. USA* **2009**, 106 (49), 20637-20640.

(30) Britt, D.; Tranchemontagne, D.; Yaghi, O.M. *P. Natl. Acad. Sci. USA* **2009**, 105 (33), 11623-11627.

(31) Furukawa, H.; Yaghi, O. M. *J. Am. Chem. Soc.* **2009**, 131, 8875-8883.

(32) Petit, C.; Huan, L.; Jagiello, J.; Kenvin, J.; Gubbins, K. E.; Bandosz, T. J. *Langmuir* **2011,** 27, 13043-13051.

(33) Rowsell, J. L. C.; Yaghi, O.M. *Angew. Chem. Int. Ed.* **2005**, 44, 4670-4679.

(34) Tranchemontagne, D. J.; Hunt, J. R.; Yaghi, O. M. *Tetrahedron* **2008**, 64, 8553–8557.

(35) Chui, S. S. Y.; Lo, S. M. F.; Charmant, J. P. H.; Orpen, A. G.; Williams, I. D. *Science* **1999**, 283 (5405), 1148 – 1150.

(36) Lowell, S.; Shields, J. E. Powder Surface Area and Porosity, 2nd Edition; Chapman and Hall: New York, NY, 1984.

(37) Petit, C.; Burress, J.; Bandosz, T. J. *Carbon* **2011,** 49, 563-572.

(38) Dunn, P.; Ennis, B. C. *Thermochim. Acta* **1971**, 3(2), 81-87.

(39) Obendorf, S. K.; Liu, H; Tan, K.; Leonard, M. J.; Young, T. J.; Incorvia, M. J. *J. Surfact. Deterg.* **2009,** 12, 43-58.

(40) Barton, A. F. M. CRC Handbook of Solubility Parameters and Other Cohesion Parameters, 2nd Edition; CRC Press: Boca Raton, FL, 1991.

(41) van Krevelen, D. W.; Hoftyzer, P. J. Properties of Polymers: Their Estimation and Correlation with Chemical Structure, 2nd ed.; Elsevier: Amsterdam, 1976.

(42) Elangovan, D.; Nidoni, U.; Yuzay, I. E.; Selke, S. E. M.; Auras, R. *Ind. Eng. Chem.* **2011**, 50, 11136-11142.

(43) Hansen, S. Hansen solubility parameters: A user's handbook; CRC Press: Boca Raton, FL, 2007.

CHAPTER 3

DEGRADATION STUDIES OF METHYL PARATHION WHEN IN CuBTC METAL-ORGANIC FRAMEWORK

3.1. Abstract

Degradation of methyl parathion adsorbed in metal-organic framework (MOF)-199 cages has been studied using nuclear magnetic resonance (NMR), Raman spectrometry, and solvent extractions. NMR was completed using solid-state ^{31}P NMR with magic-angle spinning with cross polarization or direct polarization. Results show that constitutional isomerization is the main mechanism of methyl parathion degradation within the MOF-199 framework over the 5 – 67 days of testing.

3.2. Introduction

Metal organic frameworks (MOFs) have become a research topic of wide interest in recent years. Due to their large surface areas and controllable pore sizes, MOFs have been shown to have an increased potential for selectively adsorbing chemicals and gases[1,2,3]. A MOF structure consists of metal centers connected by multifunctional linkers resulting in crystalline nanoporous materials[4,5,6], which have been proven to be useful as adsorbents and catalysts[7]. There are many ways that MOF structures can be catalytic, which include framework activity (at either the inorganic nodes or at the organic or pseudo organic linkers), encapsulation of active species, or post synthetic modification[7].

In a previous study, MOF-199, a copper(II)-benzene-1,3,5-tricarboxylate (Cu BTC) MOF composed of dimeric cupric tetracarboxylate units with a short Cu-Cu internuclear separation, was incorporated into a textile structure for potential

applications in protective clothing[8]. In that study, MOF-199 was shown to selectively adsorb methyl parathion (MP), an organophosphate pesticide and mimic for the chemical warfare agent VX, from a hexane solution[8]. It was suspected that degradation of MP was occurring within the cages of the MOF-199 because MOF-199 shows framework activity in the form of Lewis acid catalytic activity that is related to open metal sites in the Cu(II) coordination sphere[9]. However, no MP degradation products were observed during those experiments. It is well documented in the literature that Cu(II) is capable of catalyzing the hydrolysis of MP in aqueous solutions in both alkaline and acidic environments[10, 11, 12, 13]. Although the previous experiments were conducted in hexane, it is likely that water was coordinated at the MOF-199 copper sites before being introduced to the MP/hexane solution[14]. Water adsorption was confirmed with the TGA of the MOF-199 particles and the PAN/MOF fibrous membrane[8]. By having water coordinated at the copper sites of the MOF-199, it is possible that MP hydrolysis was catalyzed within the MOF-199 cages, where MP degradation products were retained.

Another possible degradation mechanism described in the literature is oxidation of MP to methyl paraoxon[15], which consists of replacing the doubly bonded sulfur with an oxygen molecule. Seger et al.[15] showed that when MP is sorbed on partially hydrated Cu(II) montmorillonite clay, the main degradation mechanism observed after 3 years was oxidation. It is possible that the environment of the Cu(II) clay could be somewhat similar to the Cu(II) environment of MOF-199. This means that both oxidation and hydrolysis are possible mechanisms of MP degradation that could be occurring upon interaction with the MOF-199 particles. If degradation is

occurring within the MOF-199 cages, further experiments will be necessary to determine the exact mechanism of degradation.

Aiming to confirm and characterize the MP degradation within the MOF-199 pores, a combination of solid-state ^{31}P nuclear magnetic resonance (NMR), Raman spectroscopy and solvent extractions were completed. Solid-state ^{31}P NMR has been used previously to study MP degradation when sorbed on both partially hydrated kaolin and montmorillonite clays of different metal forms, including Cu(II)[15]. When sorbed on these partially hydrated kaolin and montmorillonite clays, Scheme 3.1 shows the anticipated MP degradation modes, including constitutional isomerism, hydrolysis, and oxidation[15]. Raman spectroscopy was also chosen for this work because MP degradation products were found to be Raman active in areas of the spectrum that MP was not. Also, Raman can detect degradation products that do not contain phosphorous atoms, whereas ^{31}P NMR can only detect molecules that contain at least one phosphorous atom.

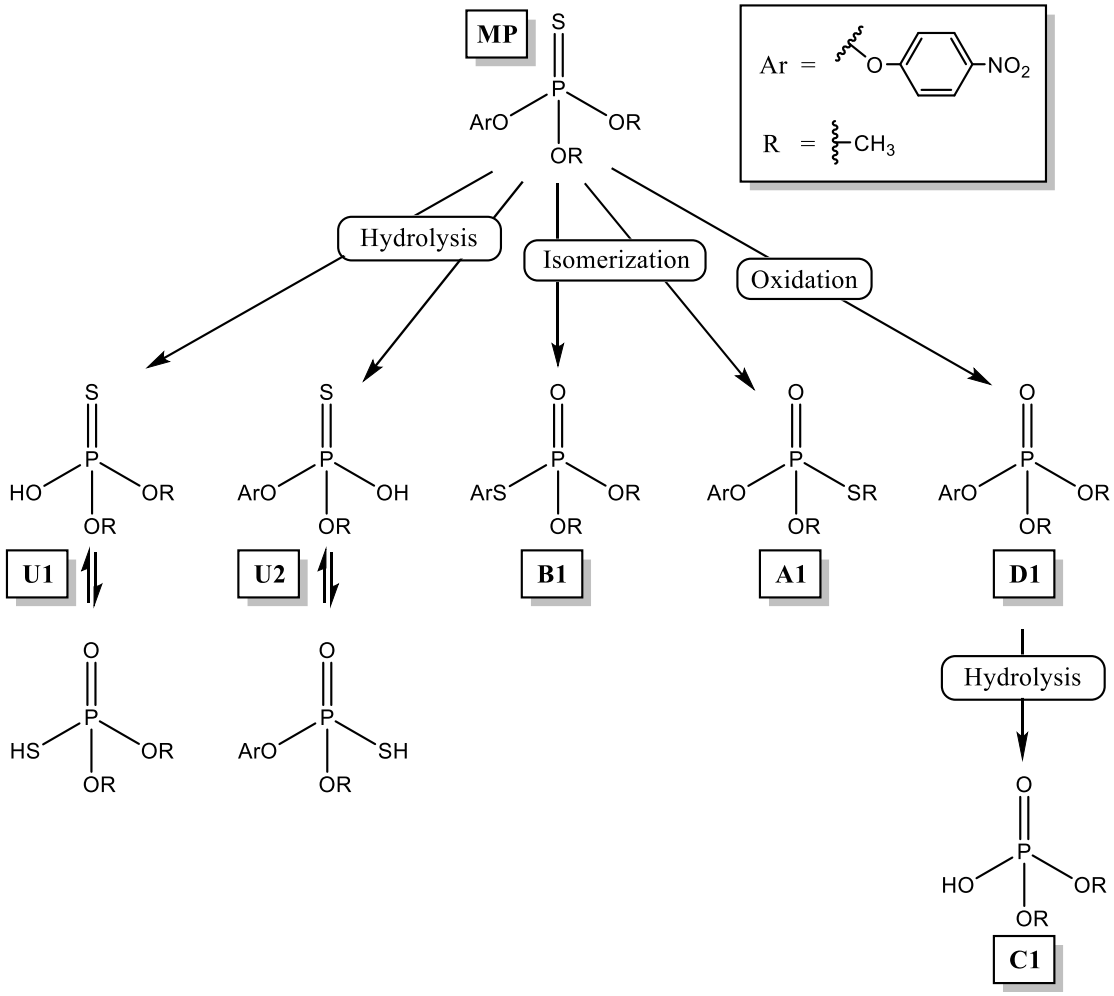

Scheme 3.1. Anticipated MP degradation modes (constitutional isomerism, hydrolysis, and oxidation) expected when sorbed on these partially hydrated kaolin and montmorillonite clays[15]. Labels relate to functional group assignment of ^{31}P NMR chemical shifts explained in Figure 3.3 and Table 3.3. Labels of A, B, C and D relate to specific phosphorous environments observed in ^{31}P NMR spectra obtained from this study, whereas U labels indicate phosphorous environments unobserved in the ^{31}P NMR spectra obtained from this study.

3.3. Materials and Methods

3.3.1. Materials

A commercially available MOF-199, Basolite C-300, was purchased from BASF (Florham Park, NJ). According to the manufacturer, Basolite C-300 has an average particle size of about 16 μm, 1500-2100 m^2/g BET surface area, 200 °C reactivation temperature, and 0.35 g/cm^3 bulk density. Methyl parathion (O,O-dimethyl-O-p-nitrophenyl phosphorothioate) (PS-94) and its degradation products (methyl paraoxon (PS-613), OOO-trimethyl phosphoric thiourate (F2570), and 4-nitrophenol (O-896)) were purchased from Chem Service Incorporated (West Chester, PA). HPLC grade hexane and HPLC grade acetonitrile were obtained from EMD Millipore Chemicals (Billerica, MA). HPLC grade water was obtained from Macron Chemicals (Center Valley, PA).

3.3.2. Methods

3.3.2.1. ^{31}P Solid State Nuclear Magnetic Resonance Spectroscopy

3.3.2.1.1. Preparation of Methyl Parathion-Loaded MOF-199 Particles for NMR Spectroscopy

10 mg of MP was dissolved in 10 mL of hexane and then introduced to 300 mg of MOF-199. This mixture was shaken for 20 min and then allowed to rest for 10 min. The MP/ hexane solution was decanted and then the MOF-199 particles were rinsed twice with 5 mL of hexane to remove excess surface MP. The particles were then vacuum dried overnight to remove excess hexane at room temperature.

3.3.2.1.2. ^{31}P solid-state NMR Spectroscopy

The particles from section 3.3.2.1.1 were then used as the sample to collect ^{31}P

solid-state NMR spectra utilizing magic angle spinning (MAS) and either cross polarization (CP) or direct polarization (DP)[15] after 1, 45, and 67 days post vacuum drying. A Varian INOVA 400 (Palo Alto, CA) was used to collect these spectra.

3.3.2.2. Sample Preparation for Raman Spectroscopy and Hexane and Water Extractions for HPLC

Three different amounts (1, 10, and 20 mg) of MP were dissolved in 10 mL of hexane and then 200 mg of MOF-199 were added to each sample and left for 27 hours. After the designated experimental time, a 1.5-mL aliquot was removed from the solution using a 5-mL syringe with Luer-Lok Tips (BD Biosciences, Franklin Lakes, NJ) and filtered using a Titan2® nylon 0.20 μm pore sized syringe filter (SUN-Sri, Rockwood, TN). Each aliquot was then transferred to a vial for high performance liquid chromatography (HPLC) analysis.

The remaining MP/hexane solution was decanted from each sample, and the remaining MOF-199 particles were then rinsed twice with 5 mL of hexane to remove excess MP from the surface of the MOF-199 particles. These particles were then vacuum dried for 10 hours at room temperature. These particles were used to obtain Raman spectra, described in section 3.3.2.3., 1 hour after vacuum drying and again after 5 days. These MP loaded MOF-199 particles were also used for water extractions after 5 and 35 days and hexane extractions after 35 days, both of which are described in section 3.3.2.4.1.

3.3.2.3. Raman Spectroscopy

Three different loadings of MP discussed in section 3.3.2.2 were used, in addition to control samples of MOF-199, MP and 4-nitrophenol. A Renishaw InVia

Confocal Raman microscope (Gloucestershire, UK) was used. The excitation wavelength was 488 nm. A 50x long-working distance objective (N. A. 0.45 for Raman imaging) was used. Normal mode calculations at the B3LYP/6-31G(d) and EDF2/6-31G(d) level were performed for expected degradation products to help identify unknown peaks using Spartan software (Wavefunction, Inc., Irvine, CA). The B3LYP and EDF2 density functional models and calculations are limited to 30 atoms. Frequencies calculated from EDF2/6-31G(d) were scaled uniformly by 0.962 to account for know systematic errors.

3.3.2.4. Hexane and Water Extractions

3.3.2.4.1. Extraction Procedures

10 mg of MOF-199 particles treated with 0, 1, 10, or 20 mg of MP were placed in a jar. 10 mL of HPLC grade hexane or HPLC grade water were added to the container. The samples were sonicated for 20 min and then left to rest for 10 min. A 1.5-mL aliquot was removed from the solution using a 5-mL syringe and filtered using the same procedure previously described. Each aliquot was then transferred to a vial for HPLC analysis. The 10-mg MOF-199 sample treated with no MP was used as a control to determine which HPLC peaks were MOF-199 induced.

3.3.2.4.2 HPLC Method

A reverse phase high-performance liquid chromatograph (HPLC) combined with a diode array UV-vis detector (DAD) from Agilent HP series 1200 (Santa Clara, CA) was used to measure the concentrations of MP. The injection volume was 20 μL. An Agilent XDB-C18 reversed phase column with 5-μm particle size, 4.6 x 150-mm dimension was used, at a temperature of 25 °C. The mobile phase consisted of 50:50

volume percent of acetonitrile and water with 0.5 v % formic acid, and the run time was 22 min. The UV-vis detector was set to scan at 280 and 320 nm and a single-quadrupole Agilent 6130 was used. MP standards and calibration curves were used to adjust for any instrument drift of the HPLC-DAD. Quantification of MP was performed using data from the DAD detector.

3.3.3. Statistical Analysis of Water Extractions

Each water extraction of the treated MOF-199 was completed in triplicate for each of the three original loadings of MP. Two-way analyses of variance (ANOVA) followed by a post hoc mean comparisons with a Tukey correction were completed using JMP 9 (SAS, Cary, NC) for each degradation product separately. These statistical tests were run to determine significant differences in the amount of each degradation product based on two variables: time between loading and extraction (5 or 35 days) and original MP loading (1, 10, 20 mg) as well as the interaction term between these two variables.

3.4. Results

3.4.1 Nuclear Magnetic Resonance

The DP-MAS ^{31}P NMR spectra for MP treated MOF-199 particles after 1, 45, 67 days of pesticide loading are shown in Figure 3.1. After 1 day, only one peak was observed at 55 ppm. After 45 days, the original peak at 55 ppm shifted to 59 ppm and had decreased in intensity. Small peaks appeared after 45 days at 30 ppm, 22 ppm, 0-1 ppm and -10 ppm. After 67 days, the intensity of the original peak at 59 ppm significantly decreased. Additionally, the small peaks that appeared after 45 days increased in intensity after 67 days. The 30 ppm and 22 ppm peaks also had the

highest intensities in comparison to the other observed peaks with chemical shifts at 59, 0 and -10 ppm. A spinning side band at about 95 ppm was also observed in the 1-day sample, but not in the 45 or 67-day samples. MP not adsorbed in MOF-199 DP-MAS ^{31}P NMR had a peak at 66 ppm. CP-MAS ^{31}P NMR spectra did not have any observable peaks.

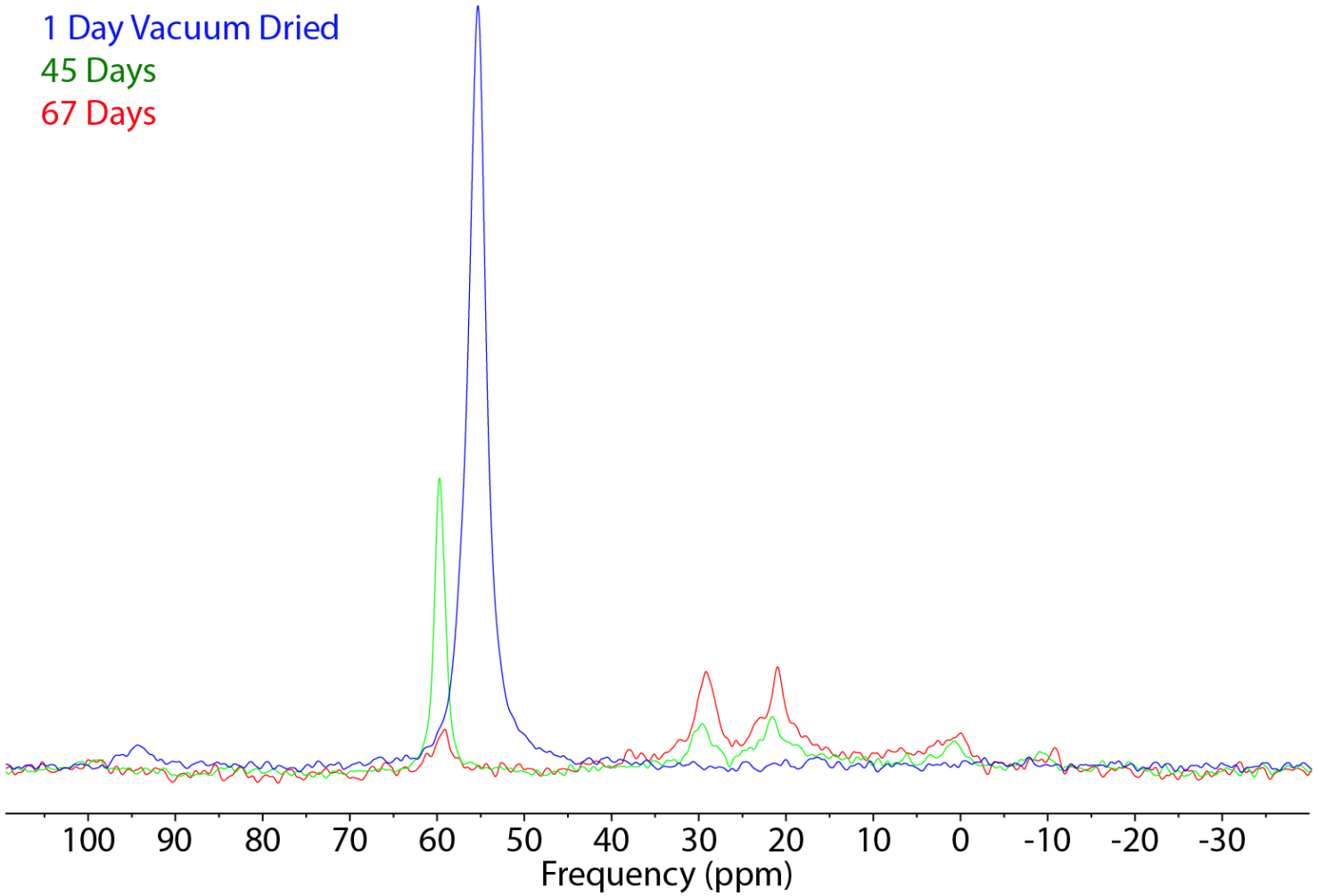

Figure 3.1. ^{31}P solid-state NMR spectra of MP loaded MOF-199 particles after 1 day vacuum dried (blue), 45 days (green), and 67 days (red).

3.4.2. Raman Spectroscopy

One hour after being removed from vacuum, the Raman spectra for the 100, 1000 and 2000 mg/L loaded MOF-199 samples all had peaks only observed in either MOF-199 or MP. Alternatively, the 5-day samples for all three loadings of MP exhibited the peaks related to MOF-199, MP, and an unidentified compound. The intensities of the peaks for different loadings were similar; so only the 2000 mg/L loading was used for further analysis. Raman spectra for MOF-199, MP, 4-nitrophenol, and the MOF-199 with a 2000 mg/L loading of MP 5 days after being removed from vacuum are shown in Figure 3.2.

The Raman spectrum for MOF-199 had peaks at 277, 448, 500, 745, 809, 827, 1005, 1219, 1387, 1450, 1463, 1542, 1613, 2651, and 3090 cm^{-1} as well as a shoulder at 819-821 cm^{-1}. The Raman spectrum for MP had peaks at 856, 1111, 1347, 1592, 3084, and a broad peak between 2849-2960 cm^{-1}. The Raman spectra for the 100, 1000, and 2000 mg/L loaded MOF particles all showed additional peaks that were not related to either MOF-199 or MP. These peaks were observed at 790, 1030, 1336, 3056 cm^{-1} and between 2901-3006 cm^{-1}.

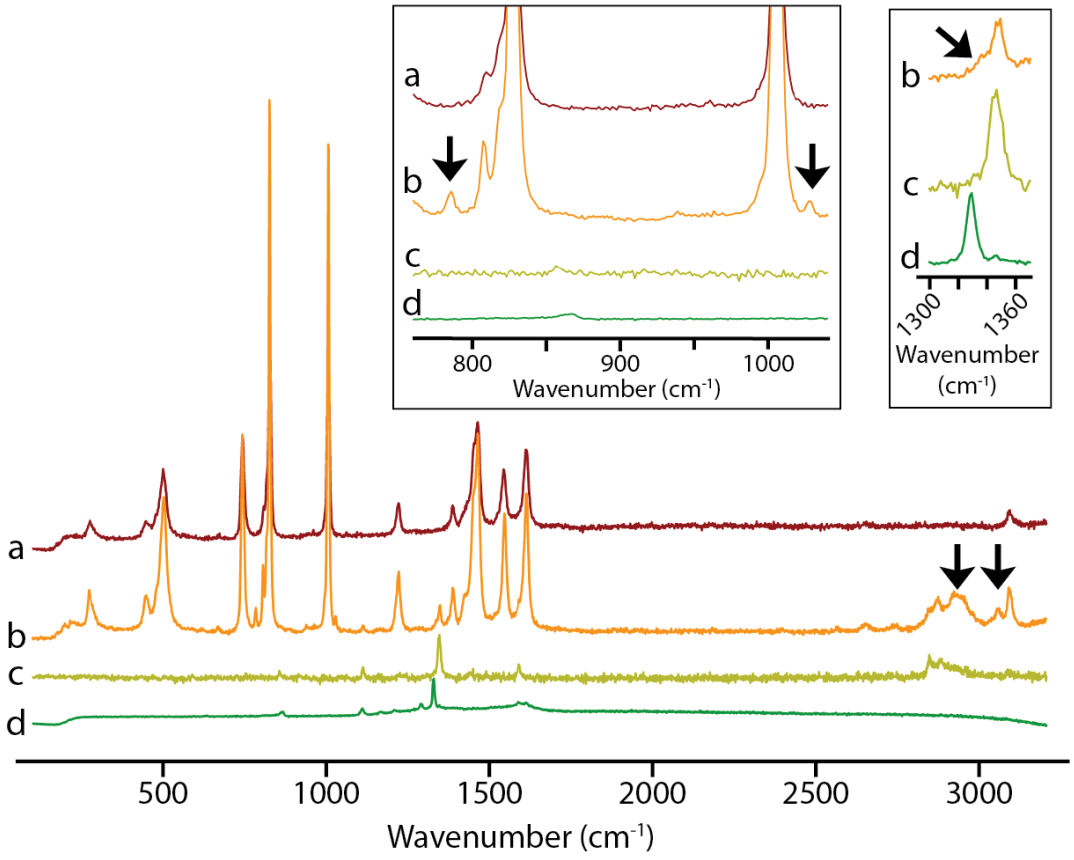

Figure 3.2. Raman spectra of (a) MOF-199 (red), (b) 2000 mg/L MP loaded MOF particles 5 days after being removed from vacuum (orange), (c) MP (yellow) and (d) 4-nitrophenol (green). Insets show select parts of the spectra between 750-1050 cm^{-1} and 1300-1370 cm^{-1}. Arrows indicate peaks only observed in the MP loaded MOF particles that are not observed in either the MOF or the MP spectra.

3.4.3. Normal Mode Calculations at the B3LYP/6-31G(d) and EDF2/6-31G(d) Level

Normal mode calculations at the B3LYP/6-31G(d) and EDF2/6-31G(d) level were performed for the possible MP degradation products, which previously had NMR frequencies assigned[15]. Calculations for 4-nitrophenol were also performed and did not show vibrations between 2900-3100 cm^{-1}, but had calculated wavenumbers at 784, 989, 1086, 1356 cm^{-1}. Select degradation products that have all the unassigned Raman peaks in their calculated spectra are shown in Table 3.1.

Table 3.1. Select results from normal mode calculations at the EDF2/6-31G(d) level for MP degradation product possibilities that most closely correspond to the unknown Raman wavenumbers observed in Figure 3.2 and are organized according to respective ^{31}P NMR chemical shifts[15]. In the chemical structures, R represents a $-CH_3$ group and Ar represents the aromatic/nitro group. Labels relate to functional group assignment of ^{31}P NMR chemical shifts explained in Figure 3.3 and Table 3.3. Labels of A, B, and D relate to specific phosphorous environments observed in ^{31}P NMR spectra obtained from this study, where as U labels indicate phosphorous environments unobserved in the ^{31}P NMR spectra obtained from this study.

		Calculated Raman wavenumbers of possible MP degradation products and observed unknown (cm^{-1})						^{31}P NMR Shift[15] (ppm)
	Structure	P-OR Stretch	Aromatic C-C Stretch	Methoxy O-C Stretch	Aromatic C-H Bend	Alkane C-H Stretch	Alkane C-H Stretch	
	Observed Unknown	785	1027		1336	2901-3006	3056	N/A
A1	O=P(OR)(SR)(OAr)	781	996	1062	1342	2951, 2974	3063, 3065	27-28
B1	$O=P(OR)_2(SAr)$	738, 811	995	1045, 1061	1327	2953, 2957	3064, 3066	22-27
B2	O=P(OR)(SAr)(OH)	752	995	1049	1329	2953	3064	25
D1	$O=P(OR)_2(OAr)$	771	996	1039, 1058	1344	2955, 2958	3066, 3068	-4.8
D2	O=P(OR)(OAr)(OH)	779	995	1067	1341	2957	3066	-4
U2	S=P(OR)(OAr)(OH)	809	1033	1046	1343	2959	3067	56
U5	$S=P(OR)(OAr)_2$	Cannot be calculated because molecule has over 30 atoms, but included because it has a P-OR and –Ar groups						58.3
U7	$S=P(OR)_2(SAr)$	774, 798	995	1036, 1049	1329	2954, 2955	3062, 3065	91

3.4.4. Solvent Extractions

After 27 hours, HPLC analysis showed that little or no MP remained in the hexane solution where 200 mg of MOF-199 were introduced for all three of the original amounts of MP (1, 10, 20 mg). Comparing the 35-day water and hexane extractions, it was observed that methyl parathion was present in both samples, but the hexane extraction showed slightly higher concentrations of methyl parathion than the water extraction. Since no additional products were observed in the hexane extraction, only the 5 and 35-day water extractions were used for further analysis. This result was expected based on previously studied solubility parameters[8].

5 and 35 days following the MP-loaded MOF-199 being removed from the test solution, water extractions were completed, resulting in the extraction of 4-nitrophenol and MP (Table 3.2). Statistically, time, original loading of MP, and the interaction between these two variables all had significant effects on the amount of MP and 4-nitrophenol extracted (Table 3.2). The 5-day water extraction showed significantly higher amounts of MP than 4-nitrophenol. However, the 35-day water extraction showed significantly higher amounts of 4-nitrophenol than MP.

Table 3.2. Amount of MP and 4-nitrophenol recovered from water extractions of 10 mg of MP loaded MOF-199 after 5 and 35 days. The original loadings of MP were 1, 10, 20 mg of MP per 200 mg of MOF. Amounts sharing the same letter superscript are not significantly different from one another. Two separate models were used to compare amounts of MP and 4-nitrophenol. The MP levels are indicated by Arabic letters, whereas the 4-nitrophenol levels are indicated by Greek letters as determined from the two-way ANOVA with the post hoc mean comparisons with a Tukey correction.

	10 mg MOF Water Extraction Amount (St. Dev.) (μg)			
	MP		**4-Nitrophenol**	
Original MP Loading Amount (mg) per 200 mg MOF-199	**5 days**	**35 days**	**5 days**	**35 days**
1	7.8 (0.3)^{b}	2.6 (0.4)^{d}	1.7 (0.0)$^{\varepsilon}$	9.3 (0.7)$^{\gamma}$
10	8.4 (0.5)^{b}	2.6 (0.7)^{d}	2.1 (0.0)$^{\delta\varepsilon}$	13.2 (0.5)$^{\beta}$
20	14.0 (0.6)^{a}	5.1 (0.4)^{c}	3.7 (0.1)$^{\delta}$	19.0 (1.4)$^{\alpha}$

3.5. Discussion

Since HPLC analysis showed that little or no MP remained in the hexane solution after 27 hours, it was determined that all of the MP was fully adsorbed by the MOF-199 particles (≥99.98% MP adsorbed). Water extractions of these particles showed MP and the production of 4-nitrophenol (Table 3.2). 4-nitrophenol is the main degradation product for hydrolysis of MP. However, introduction of water during extraction could induce hydrolysis to occur. Previously in the literature, a study was completed to study the thermodynamics of phosphate versus phosphorothioate ester hydrolysis[16]. This study completed spectroscopic investigations to determine the effect that exchanging a non-bridging oxygen atom (P=O) with a sulfur atom (P=S) within a monoester, diester, or triester had on the sission of a P-O bond. It was found that faster hydrolysis rates occur for triester phosphates than triester phophorothioates due to the entropies of activation not being large enough to overcome the increased enthalpic barrier by exchanging the doubly bonded oxygen with a doubly bonded sulfur atom. Based upon this thermodynamic study, MP and degradation products with a P=S bond should hydrolyze more slowly than methyl paraoxon and degradation products with a P=O bond. Taking this study from the literature[16] and the results from Raman and ^{31}P solid state NMR spectroscopic results into consideration, it is proposed that the increase of 4-nitrophenol in the water extraction is due to an increased amount of a MP degradation product or products that contain a P=O bond as opposed to a P=S bond and not solely due to an increased amount of 4-nitrophenol in the cages caused by the introduction of water in the extraction.

Due to the uncertainty related to the generation of 4-nitrophenol either in

MOF-199 cages or from the introduction of water, or both, ^{31}P solid-state NMR and Raman spectroscopy were used to better characterize what MP degradation products are forming inside the MOF-199 cages. MP and many of its potential degradation products have one phosphorous atom per molecule. ^{31}P solid state NMR exhibits one peak per different phosphorous atom environment, and in this case one peak per MP degradation product or MP environment. This allows for the identification of phosphorous containing degradation products while in the MOF cages without detecting or destroying the MOF.

NMR spectra obtained with DP-MAS favor mobile species while those obtained with CP-MAS favor immobile species. Since no peaks were observed in the CP-MAS NMR spectra, it is likely that the atomic level motion of MP or its degradation products is not sufficiently limited. Alternatively, in a previous study with Cu-montmorillionite, Seger et al.[15] observed that CP-MAS NMR spectra were not as intense as the DP-MAS NMR spectra. They proposed that this was due to the presence of paramagnetic Cu(II) centers. Paramagnetic atoms can negatively affect the CP dynamics from strong spin dipolar interactions preventing full ^{31}P enhancement[17]. Since no peaks were observed in this study, there is a possibility that the large concentration of Cu(II) centers in the MOF-199 severely hindered ^{31}P enhancement for the CP-MAS.

Looking at the DP-MAS ^{31}P NMR spectra, the observed frequency of a crystalline MP sample is 66 ppm, which agrees with the frequency observed in the literature[15]. The peak at 55 ppm in the vacuum dried 1-day sample is likely MP since full degradation of MP would not be expected after one day. The frequency shift from

66 ppm to 55 ppm is likely due to MP interactions with Cu(II) atoms within the MOF-199 structure. A similar shift to 58 ppm was previously reported when MP was sorbed onto Cu-montmorillonite clay[15]. However in this study, 55 ppm was the originally observed frequency for MP in the MOF-199. Vacuum drying removed absorbed water from the MOF-199 pores, which likely altered the phosphorous environment of the adsorbed MP. Over time, water was reabsorbed by the MOF-199 cages and held in close proximity to the MP likely leading to the observed shift from 55 ppm to 59 ppm for the MP peak in the 45 and 67-day sample. This peak also was reduced significantly over time and was almost completely degraded after 67 days.

Based on previous frequency assignments of MP and its degradation products[15], probable molecule assignments can be made for the 30, 22, 0-1, and -10 ppm chemical shifts (Figure 3.3, Table 3.3). Figure 3.3 shows the functional groups that are shared between structures that have the observed ^{31}P NMR chemical shifts, whereas Table 3.3 categorically labels each structure by grouping based on previously assigned ^{31}P NMR chemical shifts. Both the 30 ppm and 22 ppm peaks were present in the 45-day sample at similar intensities. The intensities of both of these peaks increased similarly in the 67-day sample. The peak at 30 ppm is likely a S,O isomer of MP with a oxygen-phosphorous double bond and a methyl sulfide group attached to the central phosphorous atom (Figure 3.3A), where the other two groups bound to the phosphorous are either a hydroxyl, methoxy, or -OAr groups, where Ar represents the 4-nitrophenyl group. Of the possibilities, **A1** is the most likely to form and therefore most probable to represent the 30 ppm peak based solely on the NMR and likelihood of formation. The peak at 22 ppm is likely another S,O isomer of MP with an oxygen-

phosphorous double bond and a –SAr group attached to the central phosphorous atom (Figure 3.3B). The other possible functional groups attached to phosphorous atom are either a methoxy or hydroxyl group. For this peak, the most likely degradation product is **B1**.

The other two peaks observed (0-1 ppm and -10 ppm) in both the 45-day and 67-day samples had a much smaller intensity than the peaks at 30 ppm and 22 ppm. Both of these peaks showed very little difference in intensity when comparing the 45-day and 67-day spectra. The 0-1 ppm peak is likely a sample that has no sulfur atoms present, has an oxygen-phosphorous double bond, and the functional groups attached to the phosphorous are methoxy, hydroxyl, or –OAr groups, basically a sulfur-free partially or fully hydrolyzed phosphate ester (Figure 3.3C). The most stable molecule for this peak is the fully hydrolyzed product phosphoric acid (**C3**). The peak observed at -10 ppm was also observed to be the largest MP degradation product after 3 years of decomposition in the previously reported study with Cu-montmorillonite clay[15]. Seger et al. assigned this peak to be methyl paraoxon (**D1**) or possibly a partially hydrolyzed form of methyl paraoxon (**C1, C2, C4**). In our study, a small intensity peak was observed at -10 ppm after 45 days and remained at a similar intensity after 67 days. This peak is also likely methyl paraoxon (**D1**) or another partially hydrolyzed form of methyl paraoxon (**D2**) (Figure 3.3D).

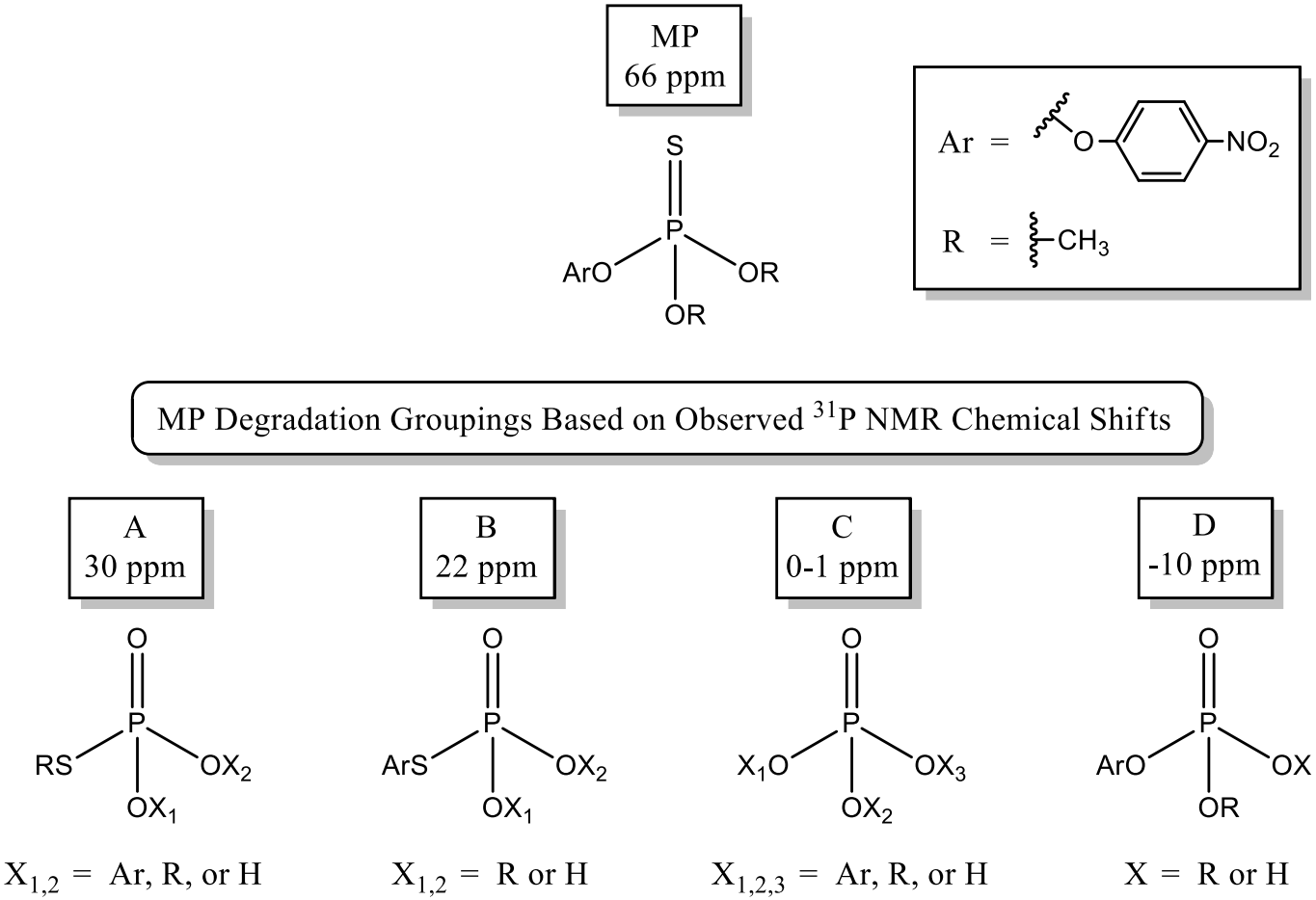

Figure 3.3. Functional group assignment of ^{31}P NMR chemical shifts at (a) 30 ppm (b) 22 ppm (c) 0-1 ppm and (d) -10 ppm to potential degradation product molecules of MP when in MOF-199 pores for 45 and 67 days based on literature assignments[15]. R represents a methyl group and Ar represents a 4-nitrophenyl group. This figure defines the nomenclature for structures shown in Scheme 3.1, Table 3.1, and Scheme 3.2.

Table 3.3. Possible MP degradation products with respective ^{31}P NMR chemical shifts[10]. Structures are organized by common ^{31}P NMR chemical shifts as observed in Figure 3.1. Structures labeled "A" represent potential degradation products that exhibit around a 30 ppm chemical shift. Those labeled "B" represent potential degradation products that exhibit around a 22 ppm chemical shift. Those labeled "C" represent potential degradation products that exhibit around a 0-1 ppm chemical shift. Those labeled "D" represent potential degradation products that exhibit around a -10 ppm chemical shift. Those labeled "U" represent potential degradation products that exhibit chemical shifts that were unobserved in the experimental ^{31}P NMR spectra from Figure 3.1. R represents a methyl group and Ar represents a 4-nitrophenyl group. This table defines the nomenclature for structures shown in Scheme 3.1, Table 3.1, and Scheme 3.2.

	Structure	Literature Assigned ^{31}P NMR Shift[15] (ppm)
MP	$S=P(OR)_2(OAr)$	66.3
A1	$O=P(OR)(SR)(OAr)$	27 to 28
A2	$S=P(OH)_3 \rightleftarrows O=P(OH)_2(SH)$	32 to 34
A3	$O=P(SR)(OAr)(OH)$	Near 30
A4	$O=P(SR)(OH)_2$	Near 30
B1	$O=P(OR)_2(SAr)$	22 to 27
B2	$O=P(OR)(SAr)(OH)$	Near 25
B3	$O=P(SAr)(OH)_2$	Near 25
C1	$O=P(OR)_2(OH)$	+4 to -2
C2	$O=P(OR)(OH)_2$	Near 0
C3	$O=P(OH)_3$	Near 0
C4	$O=P(OAr)(OH)_2$	Near 0
D1	$O=P(OR)_2(OAr)$	-4.8
D2	$O=P(OR)(OAr)(OH)$	Near -4
U1	$S=P(OR)_2(OH) \rightleftarrows O=P(OR)_2(SH)$	57.7
U2	$S=P(OR)(OAr)(OH) \rightleftarrows O=P(OR)(OAr)(SH)$	56
U3	$S=P(OR)(OH)_2 \rightleftarrows O=P(OR)(OH)(SH)$	Near 40
U4	$S=P(OAr)(OH)_2 \rightleftarrows O=P(OAr)(OH)(SH)$	41.2
U5	$S=P(OR)(OAr)_2$	58.3
U6	$S=P(OR)_3$	74.0
U7	$S=P(OR)_2(SAr)$	91

The NMR data shows that the amount of **MP** has been significantly reduced after 67-days. Based on the other NMR frequencies observed and the frequency assignments in the literature[15], it is proposed that the early mechanism of **MP** degradation is mainly constitutional isomerization, with low levels degradation via oxidation and hydrolysis. However, if time is increased to more than 67-days, it is believed that the isomerized products will hydrolyze to result in a partially hydrolyzed version of methyl paraoxon (**C1, C2, C4**).

To further explore the early degradation mechanisms of methyl parathion in MOF-199 cages, Raman spectroscopy was used. Powder Raman spectroscopy was previously completed on MP[18], resulting in peaks at 1596, 1373, 1349, 1216, 1107, and 857 cm^{-1}. These peaks were reported to correspond to the phenyl stretch, N-O stretch, C-H stretch, C-O stretch, C-N, and P-O stretch of MP, respectively. Those peak assignments were based on calculated Raman wavenumbers for methyl parathion. The wavenumbers from that previous study correspond to those observed for MP in this research, which were 1592, 1347, 1111, and 856 cm^{-1}. Based on this, the 1592 cm^{-1} is assigned to the phenyl stretch, 1347 cm^{-1} is assigned to the C-H stretch, 1111 cm^{-1} is assigned to the C-O stretch, and 856 cm^{-1} is assigned to a P-O stretch of MP. The peaks for the N-O and C-O stretches were not observed but this could be due to the low intensity of these peaks in relation to the noise and the MOF-199 peaks. These peaks in the literature were of the lowest intensity in comparison to the others and also have the least possibility for induced polarization.

Raman analysis of the vacuum dried MP-loaded MOF-199 particles completed after 1 hour and 5 days showed varying results. Since no peaks in addition to those

related to both MOF-199 and MP were observed 1 hour after removing the particles from vacuum, it was concluded that degradation does not occur within 1 hour. However, after 5 days, unassigned peaks are observed at 790, 1030, 1336, 3056 cm^{-1} and between 2901-3006 cm^{-1}. Identifying these unassigned peaks was difficult considering that all of the possible degradation products are not physically available for comparison. 4-nitrophenol was one of the expected and observed degradation products from the water extractions, but cannot be observed with ^{31}P NMR, which leaves Raman as the main method of identification. As seen in Figure 3.2, the experimental Raman spectrum for 4-nitrophenol does not match that of the unknown compound. To exclude 4-nitrophenol and other potential degradation products, normal mode calculations at the B3LYP/6-31G(d) and EDF2/6-31G(d) level results were used. Calculations showed that 4-nitrophenol did not exhibit all the Raman peaks that were shown in the unknown sample, which agrees with our experimental data for 4-nitrophenol (Figure 3.2). Specifically, there were no vibrations between 2900-3100 cm^{-1}, which are related to symmetric and anti-symmetric alkane C-H stretching. 4-nitrophenol does not have these alkane groups indicating the normal mode calculation agrees with the experimental spectra.

These calculations also helped identify proposed functional groups corresponding to each unassigned Raman peak. The vibrations between 2901-3006 cm^{-1} and at 3056 cm^{-1} respectively correspond to anti-symmetric and symmetric alkane C-H bond stretching. The 1336 cm^{-1} vibration appears to correspond to aromatic C-H bending. The 1027 cm^{-1} vibration corresponds to aromatic C-C bond anti-symmetric stretching or possibly O-C stretching of the methoxy group. And finally, the 785 cm^{-1}

vibration appears to correspond to P-O bond stretching when the oxygen is part of a methoxy group. Based on these functional group peak assignments, it was concluded that there is at least one methoxy group and an aromatic group in the unknown degradation product. Select degradation products that have both of these functional groups and therefore all the unknown Raman peaks in their calculated spectra are shown in Table 3.1.

Of the products listed in Table 3.3, **A1** and **B1** are the most likely candidates for the observed unassigned Raman peaks. This is because the chemical shifts that are associated with them were also observed in the ^{31}P NMR spectra and had the highest intensity in the NMR spectra after 45 days. However, **B2** could be equally possible. Based on the normal mode calculations, **A1** is the closest to the unassigned peaks numerically. It is also possible that more than one of these compounds is present, which would agree with the NMR data. Furthermore, evidence in the literature indicates oxidation being a longer term degradation mechanism of MP in the presence of Cu(II) montmorillonite clays[15], therefore **D1** and **D2** are not the likely compound related to the unassigned Raman peaks seen after 5 days. Also, the ^{31}P NMR spectrum does not show a significant amount of compound with the chemical shifts around -10 ppm, which likely correspond to **D1** or **D2**. In addition to this, it is unlikely that **U2**, **U5**, or **U7** are the structures that represent the unassigned Raman peaks because their corresponding chemical shifts were unobserved in any of the ^{31}P NMR spectra.

Based on water extractions, ^{31}P solid-state NMR, and Raman spectroscopy experiments, Scheme 3.2 is the proposed degradation scheme of MP when inside of the MOF-199 cages. Early degradation was attributed to constitutional isomerization

of MP (likely **A1**, **B1**, or a mixture of the two) with possible oxidation to methyl paraoxon (**D1**), based specifically on the ^{31}P NMR and Raman spectra. The water extractions also agree with the NMR and Raman analysis results. Constitutional isomerization and oxidation of **MP** leads to products that have a P=O bond instead of a P=S bond, and diesters and triesters with P=O bonds have been shown to hydrolyze more readily than their P=S counterparts[16]. As time increases, water is adsorbed into the MOF-199 pores and it is more likely that hydrolysis can occur to result in partially hydrolyzed versions of methyl paraoxon or other sulfur free molecules.

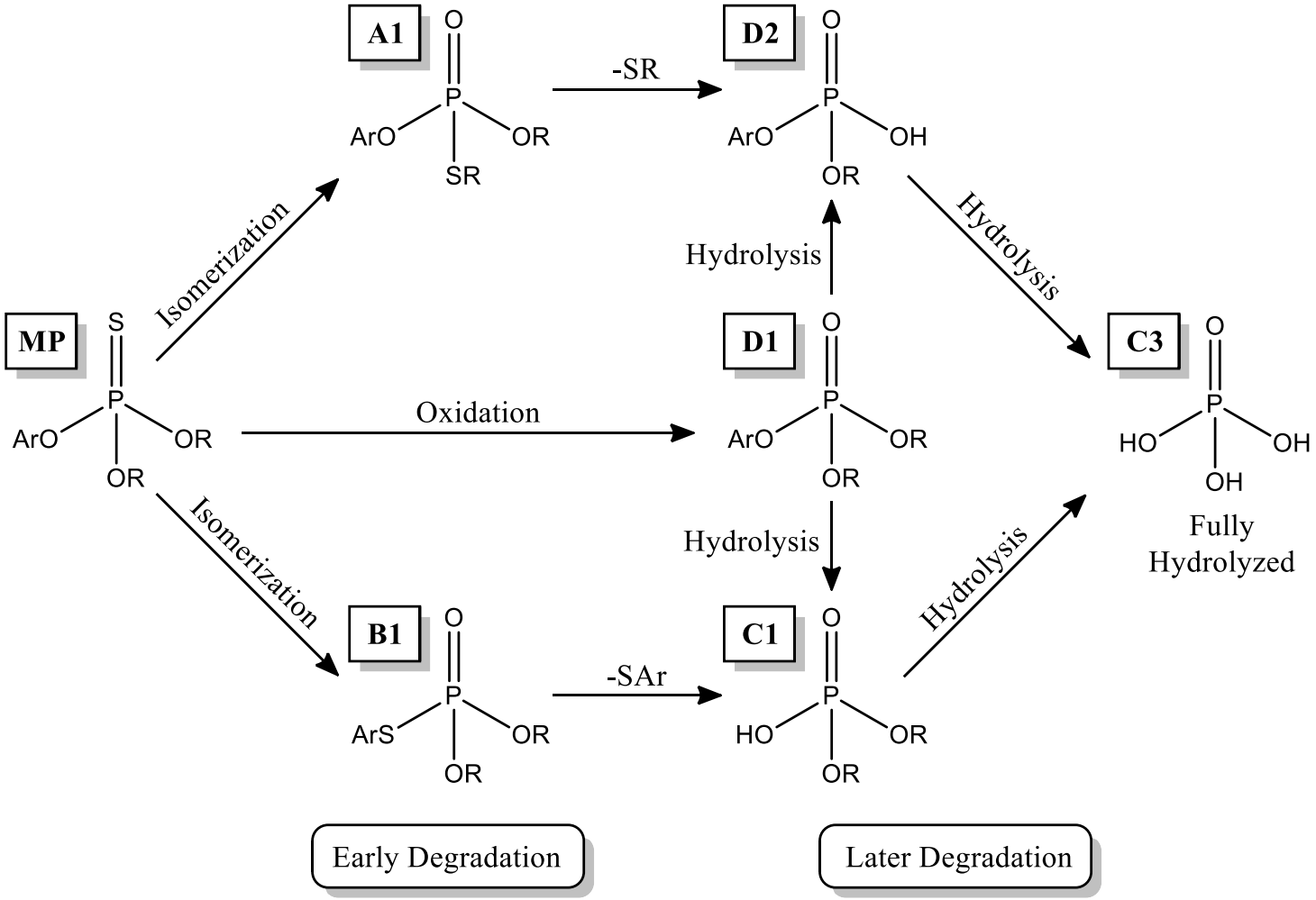

Scheme 3.2. Proposed MP degradation scheme when introduced to MOF-199 environment containing open Cu(II) active sites. Labels relate to functional gropu assignments of 31P NMR chemical shifts explained in Figure 3.3 and Table 3.3.

3.6. Conclusions

MP degradation was confirmed to be occurring when adsorbed in the MOF-199 framework. ^{31}P solid state NMR indicated that after 45 and 67 days, the main MP degradation mechanism is constitutional isomerization. Raman spectrometry after 5 days and water extractions after 5 and 35 days supported this conclusion. Normal mode calculations of Raman vibrations also showed that early degradation product(s) contain a methoxy group and a 4-nitrophenyl group. 4-nitrophenol is a common MP degradation product, but was not found to be one of the early degradation products either due to low amounts of adsorbed water or the predominance of constitutional isomerization. However, as water was adsorbed, hydrolysis of MP degradation products occurred more readily. This was concluded based on observing a significantly higher concentration of 4-nitrophenol in the 35-day water extractions than in the 5-day water extractions. Knowing that MOF-199 is capable of degrading methyl parathion, in addition to the selective adsorption of this organophosphate, demonstrates the usefulness of this MOF for potential applications in protective materials for occupational and military protective clothing.

3.7. Acknowledgements

Special thanks to Ivan Keresztes of the Cornell University NMR Facility in the Department of Chemistry and Chemical Biology for his expertise in running ^{31}P Solid state NMR experiments. Prof. Christopher Umbach and Leah McEwen were extremely helpful in the operation of the Raman spectrometer and Raman spectra interpretation. This research was funded through grants from the Cornell Agricultural Experiment Station, North Central Regional Research Project NC 170 federal formula

funds, Project NYC329801 received from Cooperative State Research, Education, and Extension Service, U.S. Department of Agriculture; College of Human Ecology; Department of Fiber Science & Apparel Design; and the American Association of Textile Chemists and Colorists. This work made use of the Cornell Center for Materials Research Shared Facilities, which are supported through the NSF MRSEC program (DMR-1120296).

3.8. REFERENCES

(1) Britt, D.; Furukawa, H.; Wang, B.; Glover, T. G.; Yaghi, O. M. *P. Natl. Acad. Sci. USA* **2009**, 106 (49), 20637-20640.

(2) Britt, D.; Tranchemontagne, D.; Yaghi, O.M. *P. Natl. Acad. Sci. USA* **2009**, 105 (33), 11623-11627.

(3) Furukawa, H.; Yaghi, O. M. *J. Am. Chem. Soc.* **2009**, 131, 8875-8883.

(4) Eddaoudi, M.; Kim, J.; Rosi, N.; Vodak, D.; Wachter, J.; O'Keeffe, M.; Yaghi, O. M. *Science* **2002**, 295, 469–472.

(5) Bordiga, S.; Regli, L.; Bonino, F.; Groppo, E.; Lamberti, C.; Xiao, B.; Wheatley, P. S.; Morris, R. E.; Zecchina, A. *Phys. Chem. Chem. Phys.* **2007**, 9, 2676-2685.

(6) Prestipino, C.; Regli, L.; Vitillo, J. G.; Bonino, F.; Damin, A.; Lamberti, C.; Zecchina, A.; Solari, P. L.; Kongshaug, K. O.; Bordiga, S. *Chem. Mater.* **2006**, 18, 1337-1346.

(7) Ranocchiari, M.; van Bokhoven, J. A. *Phys. Chem. Chem. Phys.* **2011,** 13, 6388-6396

(8) Lange, L. E.; Ochanda, F. O.; Obendorf, S. K.; Hinestroza, J. P. *Fiber Polym.* **2013,** Accepted.

(9) Schlichte, K.; Kratzke, T.; Kaskel, S. *Microporous Mesoporous Mater.*, **2004**, 73, 81–88.

(10) Hartshorn, C. M.; Deschamps, J. R.; Singh, A.; Chang, E. L. *React. Funct. Polym.* **2003**, 55, 219-229.

(11) Hartshorn, C. M.; Singh, A.; Chang, E. L. *J. Mater. Chem.* **2002,** 12, 602-605.

(12) Algiwale, T. A.; Shinde, C. P.; Purnanand *Indian J. Chem. A* **2007,** 46A, 269-272.

(13) Manzanilla-Cano, J. A.; Barceló-Quintal, M. H.; Reyes-Salas, E. O. *J. Environ. Sci. Heal. B* **2004,** B39 (4), 577-588.

(14) S. S. Y. Chui, S. M. F. Lo, J. P. H. Charmant, A. G, Orpen, I. D. Williams, *Science* **1999***,* 283, 1148-1150.

(15) Seger, M. R.; Maciel, G. E. *Environ. Sci. Technol.* **2006,** 40, 552-558.

(16) Purcell, J.; Hengge. A. C. *J. Org. Chem.* **2005,** 70, 8437-8442.

(17) Sanchez-Camazano,M.; Sanchez-Martin,M.J. Montmorillonite-catalyzed hydrolysis of phosmet. *Soil Sci*. **1983,** *136,* 89-93.

(18) Lee, D.; Lee, S.; Seong, G. H.; Choo, J.; Lee, E. K.; Gweon, D.-G.; Lee, S. *Applied Spectroscopy.* **2006,** 60 (4), 373-377.

CHAPTER 4

IN SITU SYNTHESIS OF A POLYOXOMETALATE-CuBTC METAL ORGANIC FRAMEWORK ON CELLULOSE AND REACTIVITY

4.1. Abstract

A combination of a Keggin-type polyoxometalate (POM), $[CuPW_{11}O_{39}]^{5-}$, with a metal-organic framework (MOF), MOF-199 (HKUST-1) was successfully self-assembled on a cellulose substrate (cotton) with a newly developed room-temperature process. This material was found to effectively remove 2.75 times as much of a target organophosphate toxin, methyl parathion, from a hexane solution as MOF-cotton and cotton control samples after 2 h. The combination of the catalytic activity of the POM and the adsorption properties of the MOF both immobilized on a textile is ideal for potential applications in protective self-decontaminating materials. In addition to this, hydrophilicity of the fabrics is maintained, which leads to a material that maintains the thermal comfort of cotton.

4.2. Introduction

Organophosphates (OPs) are a type of organic phosphorous compound that are used as neurotoxic pesticides and chemical warfare agents. Humans are susceptible to OPs due to their ability to bind to acetylcholine esterase. When this binding occurs, nerve impulses are disrupted which prevents the normal functions of nerve cells[1]. A common exposure route is through dermal adsorption. Creating materials that have the ability to increase human protection from dermal adsorption of OPs while maintaining thermal comfort has become an important research topic.

Potential approaches for adsorbing and/or detoxifying organophosphates have been widely studied. Some of these solutions include enzymatic biodegradation[2], electrochemical[3], catalytic oxidation[4], atmospheric pressure plasma[5], photolytic[6], and destructive adsorption[7] methods. Hydrolysis of OPs has been a widely used mechanism of detoxification using TiO_2[8], MgO[7,9], nano-meter sized Al_2O_3[10,11], ZnO[12], Au/TiO2[13], activated carbons[14], polymers[15], and mesoporous silica[16]. Adsorption and subsequent degradation of organophosphates using clays[17,18], soil components[19], and zeolites[20,21] have been studied. Metals, metal oxides, and metal-organic frameworks (MOFs) degradation and/or adsorption of OPs have been a focus in this lab with respect to textiles for many years[7,22].

MOFs are of interest due to their large surface area and controllable pore size and have been shown to selectively adsorb chemicals and gases[23,24,25] including organophosphates[23]. MOFs are crystalline nanoprous materals composed of metal clusters connected by multifunctional organic linkers[26,27,28]. MOFs have also been recently shown to be useful in catalysis[29-35]. Catalysis with MOFs can be achieved in one of three ways: (1) framework activity at either the inorganic clusters or at the organic or pseudo-organic linkers, (2) encapsulation of active species, or (3) post-synthetic modification[36]. MOF-199 has been shown to act catalytically as a Lewis acid due to the open metal sites on the Cu(II) coordination sphere[37]. MOF-199 is a copper(II)-benzene-1,3,5-tricarboxylate (Cu BTC) MOF composed of dimeric cupric tetracarboxylate units that exhibt a short Cu-Cu internuclear separation[38] with the chemical formula of $[Cu_3(C_9H_3O_6)_2]$.

In addition to the open Cu(II) metal sites in MOF-199, there is potential for

encapsulation of other active agents in the cages. This could potentially increase the functionality of the MOF structure by combining framework activity of the inorganic cluster with encapsulation of a reactive agent. One class of materials that has recently been incorporated into MOF structures is polyoxometalates (POMs). POMs are very promising materials for oxidative self-decontamination of chemical threats such as chemical and biological warfare agents and pesticides. The POM catalyst is regenerated by ambient air following oxidation of the threat compound, ideally to a less toxic compound[39,40]. Polytungstates with 3d metals, such as Cu, substituted at the surface positions are a class of POM that are particularly useful for air-based oxidations[41-45]. There have been multiple reports of encapsulating POMs within the cage structure of the MOF[39,46-55]. Some of these efforts resulted in materials that possessed the selective adsorption of the MOF with the catalytic activity of the POM.

More specifically, MOF-199 has been combined with a Keggin-type polyoxometalate with a chemical formula of $[CuPW_{11}O_{39}]^{5-}$ through physical encapsulation[39]. This encapsulation is possible due to the close matching of POM diameter in relation to the MOF-199 cage channels. This was shown to be a favorable combination of materials due to their reported increased hydrolytic stability and improved catalytic effects of the POM-MOF over the MOF or the POM alone. This POM-MOF was shown to catalytically oxidize hydrogen sulfide to elemental sulfur via air-based oxidation likely at the Cu centers in the POM[39].

With regard to protective clothing or textiles, the benefit of combining these two materials on a textile fabric not only improves the catalytic self-decontaminating properties of the textile by incorporating the POM, but also allows for possible

adsorption of potentially harmful oxidation products by incorporation of the MOF structure[40] to create a multifunctional material with potential applications in protective clothing. Here, we present a room temperature self-assembling method of this previously reported POM-MOF structure on a cellulose substrate. Cotton was chosen as a model for cellulose, which has many available active hydroxyl sites that allow for it to be easily modified. Cellulose has been found to be one of the most plentiful renewable polymers in nature and has many industrial applications[51].

4.3. Experimental Section

4.3.1. Materials

POM, $K_5[CuPW_{11}O_{39}]$, was provided by Craig Hill from Emory University (Atlanta, GA). Desized and unbleached cotton print cloth (Style #: 400U, Lot #: 1722) was purchased from Testfabrics, Inc. (West Pittston, PA). Copper (II) nitrate trihydrate, trimesic acid, and sodium chloroacetate were purchased from Sigma-Aldrich (St. Louis, MO) and used without further purification. Sodium hydroxide was from Mallinckrodt (Hazelwood, MO). HPLC grade hexane, HPLC grade acetonitrile, and N,N-dimethylformamide (DMF) were from EMD Millipore (Gibbstown, NJ). Ethanol (200 proof) was from Pharmco Products (Brookfield, CT). All water used was filtered using a Milli-Q Advantage A10 system and a LC-pak™ polisher from Millipore (Billerica, MA). Basolite C-300 (BASF, Florham Park, NJ), a commercially available MOF-199, was used as a standard for XRD and IR analysis. Methyl parathion and its degradation products, methyl paraoxon (PS-613), OOO-trimethyl phosphoric thiourate (F2570), and 4-nitrophenol (O-896) were purchased from Chem Service Incorporated (West Chester, PA)

4.3.2. Instrumentation for Morphological and Chemical Characterization

Field emission scanning electron microscopy (FE-SEM) was completed using a LEO 1550 FE-SEM from Carl Zeiss, Inc. (Thornwood, NY) with a Bruker AXS X-Ray Microanalysis Quantax system (Berlin, Germany). FE-SEM image analysis of particle size was performed using ImageJ (National Institutes of Health, Bethesda, MD) by averaging a total of 90 particle size measurements from 3 different images (30 measurements per image) for each sample. A Nicolet Magna IR 560 spectrometer FTIR (Thermo Fisher Scientific Inc., Waltham, MA) with a MIRacle Attenuated Total Reflectance (ATR) attachment (PIKE Technologies, Madison, WI) was used to obtain all spectra. A Scintag Theta-Theta X-ray Diffractometer (XRD) was used to analyze the crystal structure by scanning from 3-60 degrees at 2.5 degrees per min. IMR Test Labs (Ithaca, NY) determined the elemental weight percent of copper and tungsten. Contact angle was determined through wetting force using a KSV Sigma 701 tensiometer from Biolin Scientific, Inc. (Linthicum Heights, MD) by averaging 240 measurements for each sample. Thermogravimetric analysis (TGA) was completed using a TGA Q500 from TA Instruments (New Castle, DE) ramping from 20 °C to 1000 °C at 10 °C/min.

4.3.3. Fabric Preparation

4.3.3.1. Carboxymethylation of Cellulose

To assemble the MOF structure on the cotton fiber, an anionic site was created on which the Cu ions could be bonded. This was acheived by creating carboxymethylated cellulose using the following procedure[52] that is based on a classic reaction between chloroacetate salt and cellulose using sodium hydroxide as a catalyst.

Four 2x2-inch untreated cotton specimens were submerged in 150 mL of water containing 30 g sodium hydroxide for 10 min. The specimens were removed and padded dry and then heated to 45 °C for 12 min. Then, the specimens were soaked in 150 mL of water containing 30 g sodium chloroacetate for 5 min to create the carboxylate group on the cellulose. The specimens were again padded dry and then heated to 85 °C for 30 min to cure. Water was then used to vigorously wash the specimens to remove any unreacted materials before acidification with 150 mL of a 2 g/L acetic acid aqueous solution. One more wash with water was done before air-drying the specimens.

4.3.3.2. Preparation of POM-MOF-cotton and MOF-cotton Fabrics

The synthesis of the POM-MOF on the surface of the cellulose substrate (POM-MOF-cotton) was based on two modified methods from the literature[53,54]. First, three separate solutions were made: 800 mg of trimesic acid was dissolved in 12 mL ethanol, 1.00 g $CuNO_3 \bullet 3H_2O$ was dissolved into 14 mL ethanol, and 800 mg $K_5CuPW_{11}O_{39}$ was dissolved in 14 mL H_2O. All three solutions were sonicated for 30 min. 250 mg of carboxymethylated cotton was added to the $CuNO_3 \bullet 3H_2O$/ethanol solution and left to stir for 24 h. Then, over 10 min, the following solutions were added to the $CuNO_3 \bullet 3H_2O$/ethanol solution dropwise in this order: 7 mL of POM/water, 6 mL of trimesic acid/ethanol, 7 mL of POM/water, and finally 6 mL of trimesic acid. This was left to stir for 45 h. Fabric was removed from the reaction vessel and stirred in 20 mL of water for 3 h, followed by 20 mL of DMF for 3 h, and finally ethanol for 3 h to remove any unattached reaction products. The fabric was then vacuumed dried overnight at room temperature. MOF-cotton samples were

prepared with the same procedure except the POM was not added to the water. Proposed mechanism for POM-MOF-cotton formation based on this procedure is shown in Scheme 4.1.

The solvent system was chosen to solubilize both the POM and trimesic acid. In the previously reported room temperature synthesis of MOF-199 on cellulose[53,54], DMF, ethanol, and water were used in equal parts to encourage self-assembly of the MOF structure. Trimesic acid is not very soluble in water, so increasing the percent of water in the solvent system was to be avoided. The POM, however, is not very soluble in DMF, and therefore, it was replaced with ethanol for these experiments.

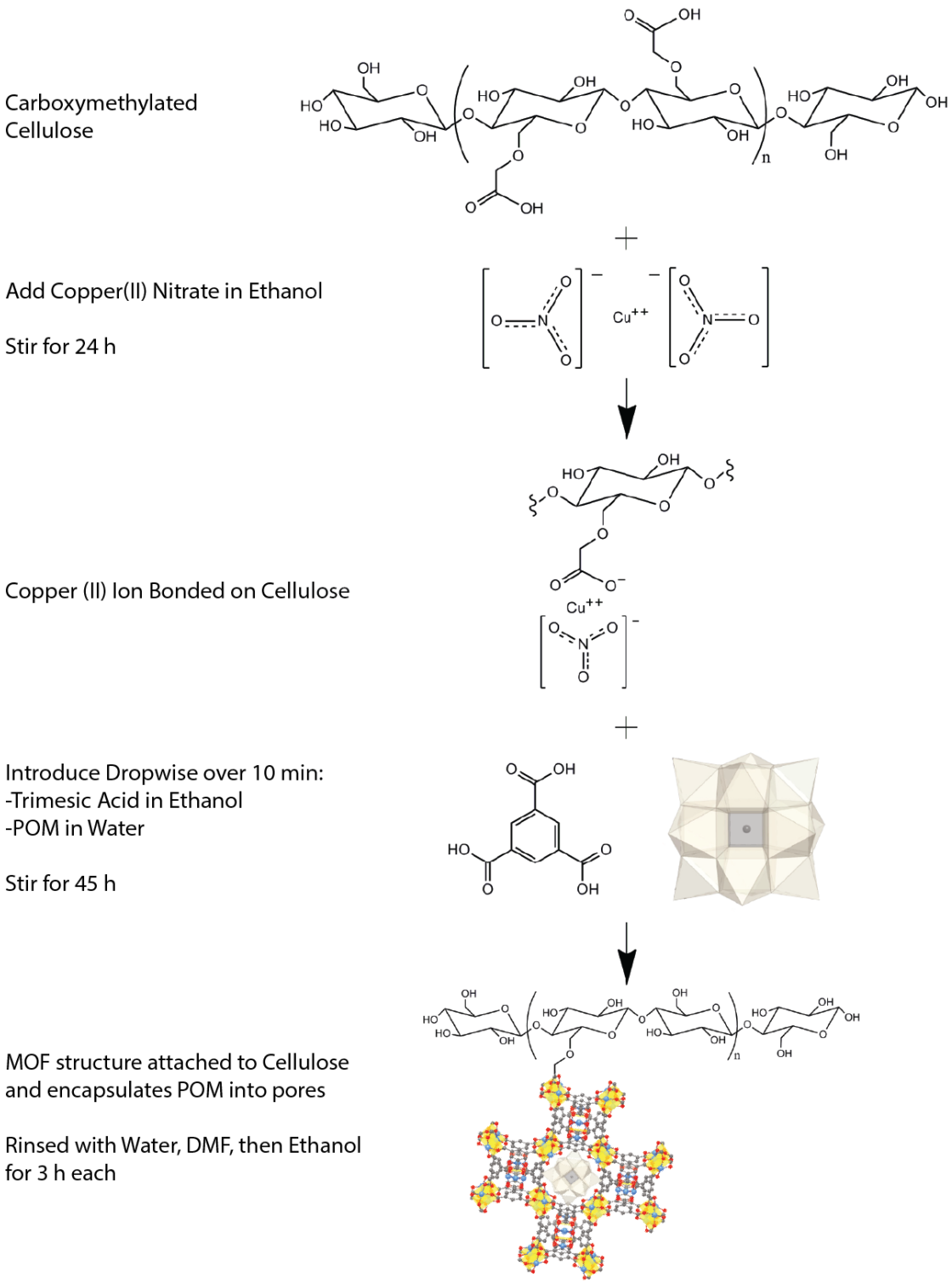

Scheme 4.1. Procedure and proposed mechanism for POM-MOF formation on carboxymethylated cellulose. POM and POM-MOF crystal structure images are from Song et al[39], which was published by ACS Publications.

4.3.4. Fabric Performance

4.3.4.1. Testing Procedure

Four replicates of three fabric types (cotton, MOF-cotton, POM-MOF-cotton) were cut into 1.5 cm diameter circles. The fabric specimens for all three of the fabric types were heated to 120 °C for 1 h to remove water. Each fabric specimen was submerged in 100 mL of a 20 mg/L methyl parathion/hexane solution and put on a New Brunswick Scientific Innova 2300 platform shaker (Edison, NJ) at 200 RPM. 2 mL aliquots were removed from each reaction vessel after 0.5, 1, 2, 6, 12, and 24 h, filtered with a Titan2® nylon 0.20-µm pore sized syringe filter (SUN-Sri, Rockwood, TN), and transferred to HPLC vials for analysis. Amount of methyl parathion (mg) was calculated from HPLC data acquired using the method in section 3.3.4.2. To account for sampling and evaporation of hexane during testing, a set of four 100 mL controls of 20 mg/L methyl parathion/hexane solutions were used. These control samples were sampled at identical times to the test specimens to determine the hexane evaporation for use in correcting the concentration of methyl parathion for any observed evaporation of solvent. Test specimen concentrations were adjusted appropriately for determination of methyl parathion amount in the test solutions.

4.3.4.2. HPLC Method

A reverse phase high-performance liquid chromatograph (HPLC) attached to a diode array UV-vis detector (DAD) from Agilent (Santa Clara, CA) HP series 1200 was utilized to measure methyl parathion concentration. The injection volume was 20 µL. An Agilent XDB-C18 reversed phase column with 5-µm particle size, 4.6 x 150-mm dimension was used, at a temperature of 25 °C. A 50:50 volume ratio of

acetonitrile and water with 1 v % formic acid was used as the mobile phase. The run time for each sample was 22 min. The UV-vis detector was set to scan at 230, 280 and 320 nm. Methyl parathion standards and calibration curves were used to adjust for drift of the HPLC-DAD instrument and to calculate the amount of methyl parathion. Quantification of methyl parathion concentration was performed using data from the DAD detector.

4.3.4.3. Statistical Analysis of Methyl Parathion Removal

Each experiment was performed with four replicates. Two-way analyses of variance (ANOVA) followed by a post hoc mean comparisons with Tukey correction were completed using JMP 9 (SAS, Cary, NC). The statistical tests were run to determine if significant differences were evident between the amounts of methyl parathion removed based on two variables: reaction time (0.5, 1, 2, 6, 12, and 24 h) and substrate type (POM-MOF-cotton, MOF-cotton, and untreated cotton).

4.4. Results

4.4.1. Optical Fabric Evaluation

First, the fabric specimens were evaluated optically after being washed (Figure 4.1). There was a marked difference in color between POM-MOF-cotton and MOF-cotton fabric samples. The POM-MOF-cotton exhibits a deeper aqua blue color in comparison to the lighter blue of the MOF-cotton sample.

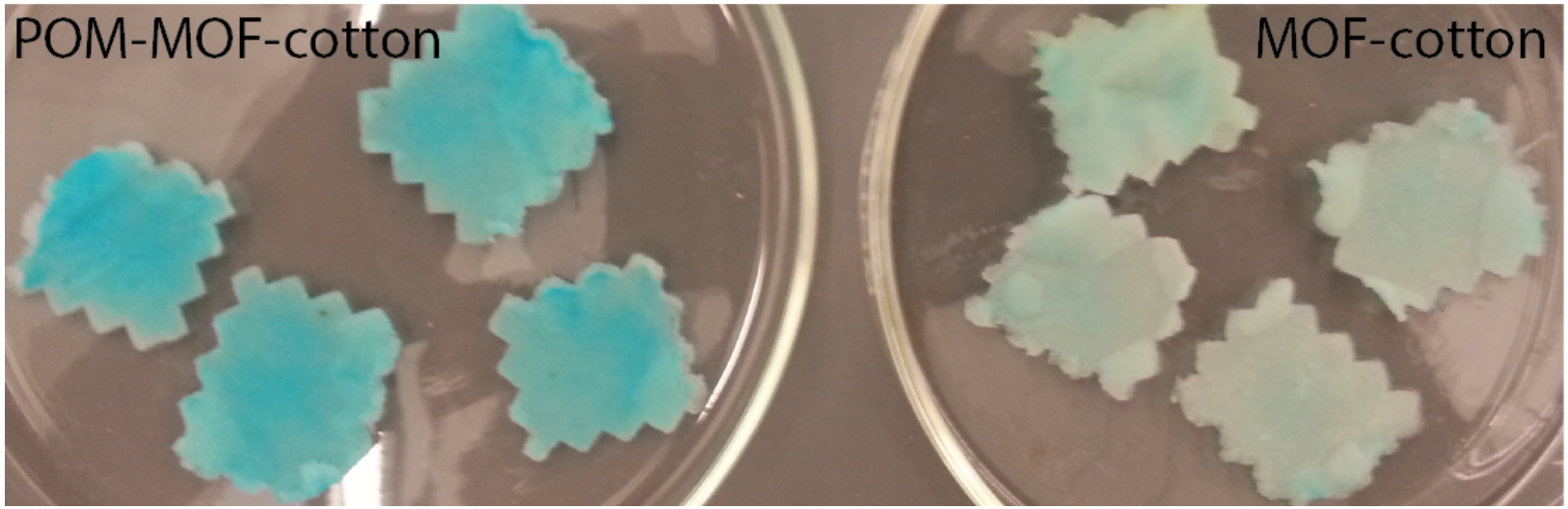

Figure 4.1. Optical image of POM-MOF-cotton (left) and MOF-cotton fabrics (right) immediately after washing. Specimen are approximately 1x1 inch in area.

4.4.2. FE-SEM with X-ray Energy Dispersive Analysis

The MOF-cotton crystals clearly have an octahedral shape, while the microstructures in POM-MOF-cotton sample seem to have more of a truncated octahedral shape (Figure 4.2). Also, while performing image analysis of three different FE-SEM images for both MOF-cotton and POM-MOF-cotton, significantly different particle sizes were observed between the two sample types. The microstructures grown on the POM-MOF-cotton samples had an average particle size of 1.51 μm with a standard deviation of 0.68 μm, whereas the microstructures grown on the MOF-cotton samples had an average particle size of 0.52 μm with a standard deviation of 0.30 μm. Both of these observed crystal sizes were much smaller than 20-25 μm, which was the size reported from a typical solvothermal synthesis[55].

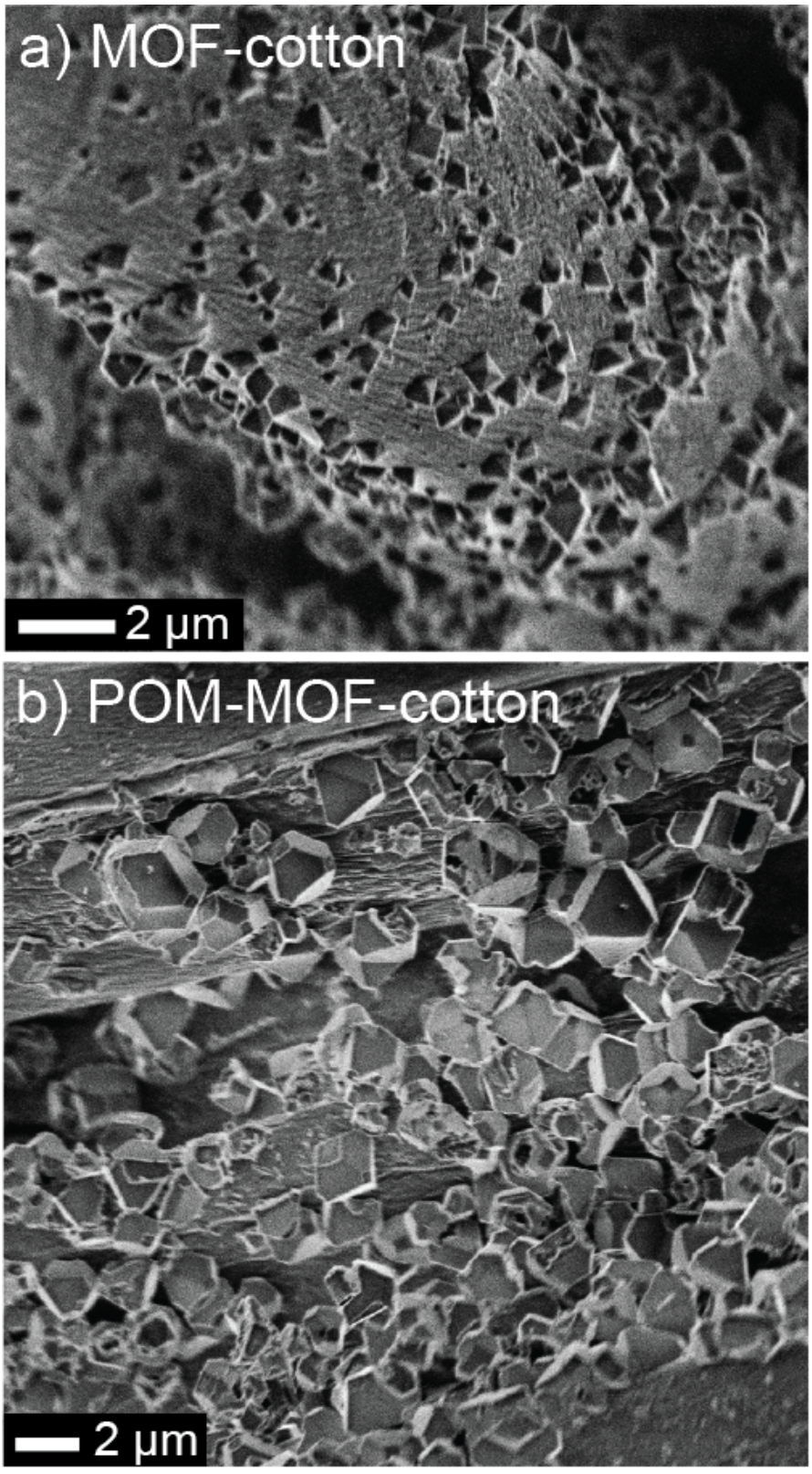

Figure 4.2. FE-SEM of (a) MOF-cotton and (b) POM-MOF-cotton.

X-ray energy dispersive analysis with a primary energy at 7 keV was used to evaluate the presence of copper and tungsten in the microstructures assembled on the fiber surfaces for the MOF-cotton and POM-MOF-cotton specimens. The M_α adsorption edge for tungsten is at 1.774 keV. At this energy, a small peak was observed in the POM-MOF-cotton fibers (2.1 counts) but not for the MOF-cotton fibers (0 counts). Both samples exhibited a copper L_α peak at 0.930 keV.

4.4.3. Metal Weight Percent Quantification

To quantify the amount of MOF and POM that were present in each fabric sample, inductively coupled plasma atomic emission spectroscopy (ICP-AES) was completed by IMR Test Labs to determine the weight percent of elemental copper and tungsten present (Table 4.1). These data show that a small amount of copper is present in the original cotton specimen, but extremely little or no tungsten is present. The weight percent of Cu is significantly higher for the MOF-cotton and the POM-MOF-cotton than the cotton control. When comparing the MOF-cotton to the POM-MOF-cotton, there is definitely more copper and tungsten in the latter. The POM-MOF-cotton had 42 times more tungsten present than the MOF-cotton.

Table 4.1. Reported weight % of copper and tungsten in the three fabric sample types.

Element	**Cotton (%)**	**MOF-cotton (%)**	**POM-MOF-cotton (%)**
Cu	0.04	0.88	1.30
W	<0.01	0.01	0.42

4.4.4. Infrared Spectroscopy

To characterize the functional groups in the materials, infrared spectrometry was utilized. Figure 4.3 shows the infrared spectra for POM before incorporation, commercial MOF, POM-MOF-cotton, MOF-cotton, and untreated cotton. The MOF has significant IR peaks at 728, 760, 1369, 1446, 1646 cm^{-1}. These peaks are observed in the POM-MOF-cotton, and with less intensity in the MOF-cotton. The peaks at 1446 cm^{-1} and 1646 cm^{-1} are likely due to the C-C stretching of the aromatic ring. The 1369 cm^{-1} peak is likely due to C-O stretching of the carboxyl groups. These peaks are also reported in the literature[39].

Peaks that are not related to the MOF or to cellulose were not clearly discernable. Specifically, peaks related to the POM molecules could not clearly be detected in the POM-MOF-cotton sample. However, in the POM-MOF-cotton spectra there is a very small broad peak between 770-815 cm^{-1} that corresponds to the peak with the largest absorption in the POM spectrum, which has a maximum adsorption at 785 cm^{-1} as seen in Figure 3.3 and in the literature[39].

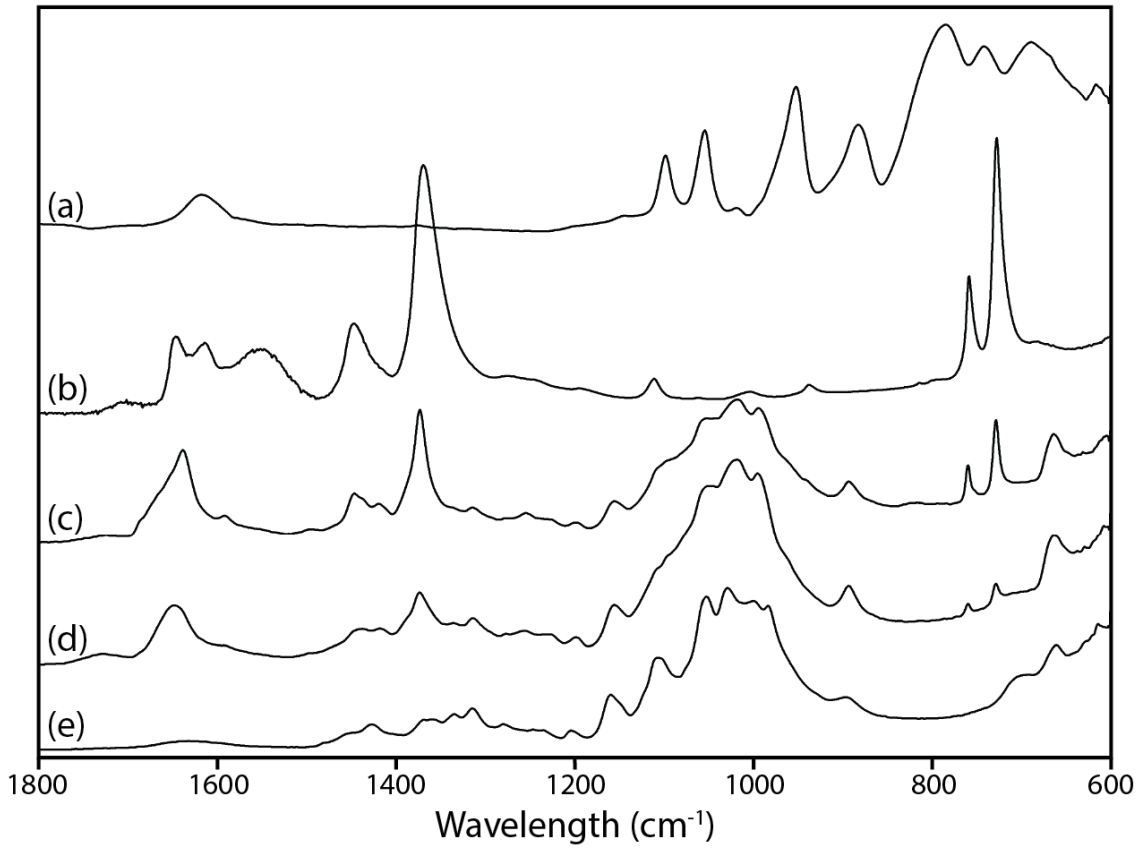

Figure 4.3. Infrared spectra of (a) POM, (b) MOF-199, (c) POM-MOF-cotton, (d) MOF-cotton, and (e) untreated cotton.

4.4.5. X-Ray Powder Diffraction

To analyze the crystalline structure of the microstructures formed on the cellulose substrate, X-ray powder diffraction patterns of MOF-199, POM-MOF-cotton, MOF-cotton and, carboxymethyl cotton, untreated cotton were obtained (Figure 4.4). The MOF-199 XRD powder diffraction pattern exhibits major 2θ peaks at 5.7, 6.6, 9.5, 11.5, 13.4, 19.0, 26.0, and 29.3. Of these MOF-199 peaks 5.7, 6.6, 9.5, 11.5, and 29.3 do not overlap with the diffraction pattern for carboxymethyl cotton, and will be most useful for identification of MOF formation on the substrate. In the POM-MOF-cotton diffraction pattern, all of the major peaks including those that overlap with the carboxymethyl cotton pattern are easily observed, but they have much lower intensities than in the MOF-199 diffraction pattern. In the MOF-cotton diffraction pattern, only the 2θ peaks at 6.6 and 11.5 are easily observed, but they have lower intensities than the related peaks for POM-MOF-cotton and MOF-199. Also for MOF-cotton, peaks were dectected at 2θ of 9.5 and 13.4, which correspond to the main diffraction pattern peaks of MOF-199 that do not overlap significantly with the carboxymethyl cellulose diffraction pattern. POM XRD peaks are not observed in the POM-MOF-cotton, indicating that the POM is not crystalline within this fabric specimen.

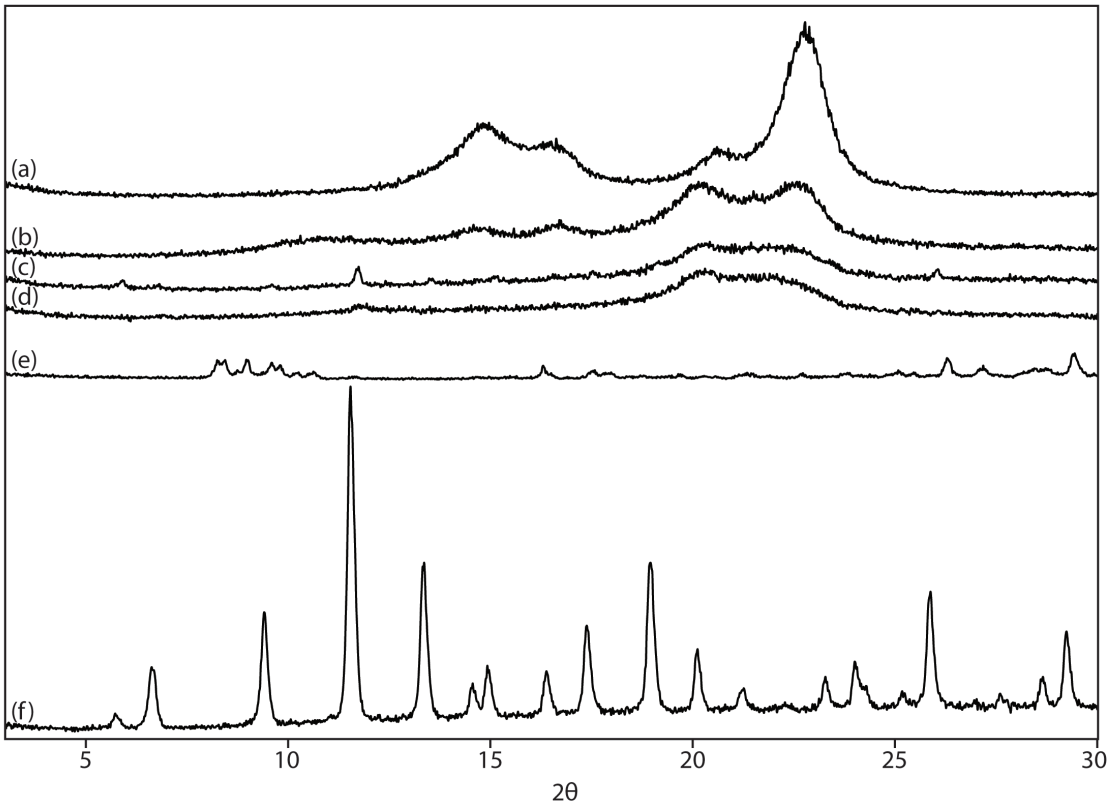

Figure 4.4. X-Ray diffraction patterns of (a) untreated cotton, (b) carboxymethylated cotton, (c) POM-MOF-cotton, (d) MOF-cotton, (e) POM, (f) MOF-199. The most prominent peaks of the MOF-199 structure can be clearly seen in the POM-MOF-cotton sample and to a lesser extent in the MOF-cotton specimen. POM peaks are not observed in the POM-MOF-cotton.

4.4.6. Wetting Force Measurements

To determine the effect of the MOF and POM materials on the hydrophilicity of the cotton substrate, contact angles were determined using wetting force measurements (Table 4.2). The POM-MOF-cotton had the smallest contact angle, followed by the MOF-cotton, and then the untreated cotton sample. The lowest average contact angle corresponds with highest hydrophilicity.

4.4.7. Thermogravimetric Analysis

Thermogravimetric analysis was used to determine if there was a significant difference in water absorption between substrate types (Figure 4.5). After heating to 100 °C, the carboxymethylated cotton, the POM-MOF-cotton, and the MOF-cotton samples lost between 6.3-7.6 % weight. After heating to 1000 °C, the carboxymethyl cotton had 0 wt% remaining, the MOF-cotton had 2.7 wt% remaining, the POM-MOF-cotton had 8.2 wt% remaining, and the untreated cotton had 5.7 wt% remaining.

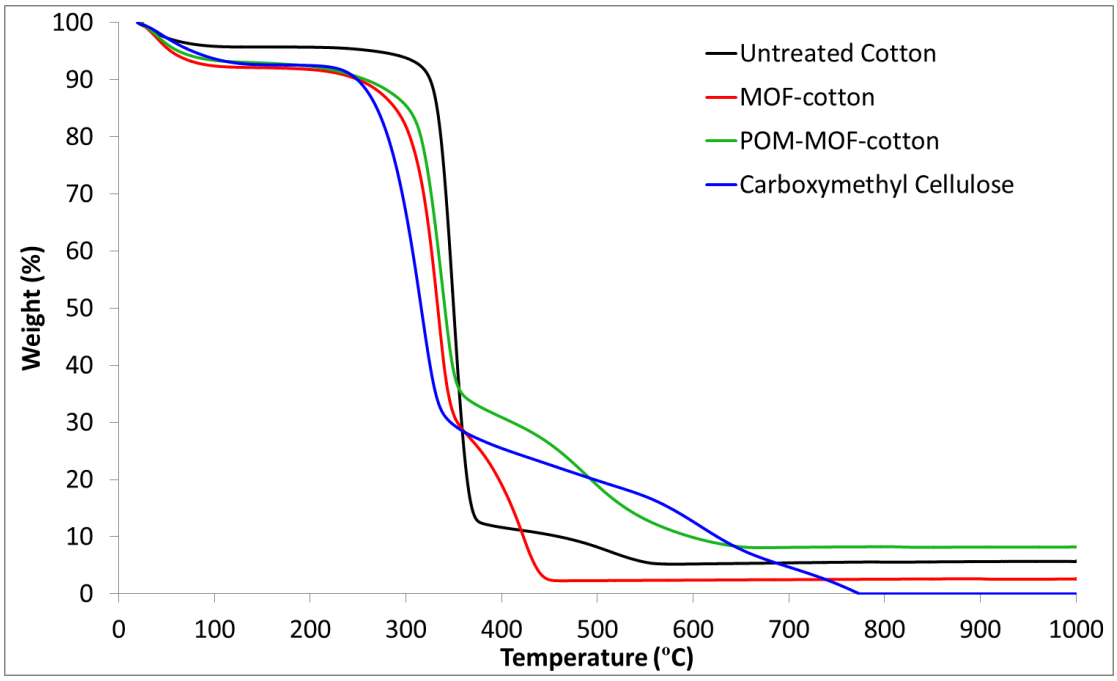

Figure 4.5. TGA thermograph showing weight loss (%) for the three specimen types based on temperature (°C). Untreated cotton is black. MOF-cotton is red. POM-MOF-cotton is green. Carboxymethylated cellulose is blue.

4.4.8. Toxin Removal and Decomposition

When introducing the three types of fabrics to 2 mg of methyl parathion in a hexane solution there were significant differences in the amount of methyl parathion removed from solution (Figure 4.6), and no degradation products were observed in the test solution by HPLC. Based on Figure 3.6, the POM-MOF-cotton sample appeared to remove more methyl parathion than either the MOF-cotton or the untreated cotton. After 6 h, no further significant amounts of methyl parathion were removed by any of the three substrate types.

Table 4.2. Contact angle for the three fabric sample types. Standard deviations are in parenthesis.

Sample	**Contact Angle (°)**
POM-MOF-cotton	11 (12)
MOF-cotton	22 (11)
Untreated cotton	38 (6)

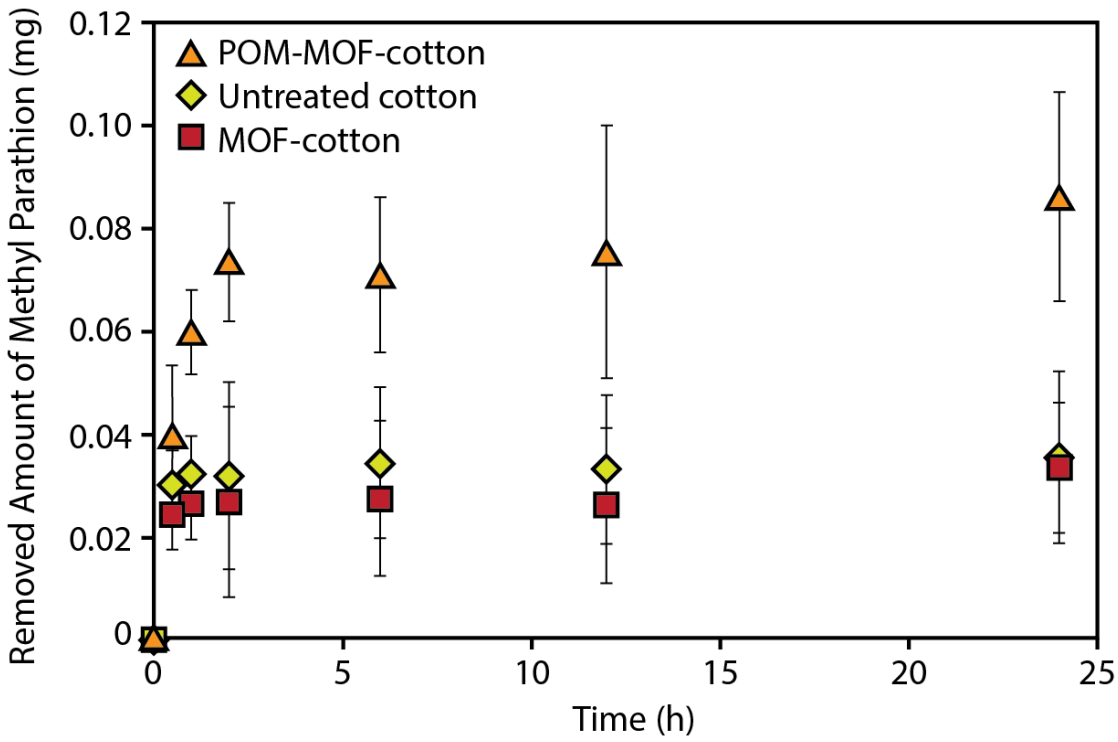

Figure 4.6. Removed amount of methyl parathion (mg) over time for the three different substrate types (POM-MOF-cotton, MOF-cotton, and untreated cotton). Error bars indicate the standard deviation in both directions. These specimens all were normalized by area of fabric. Each specimen had an area of 1.77 cm^2.

ANOVA testing was completed using three different model effects, which were reaction time (0.5 - 24 h), substrate type (POM-MOF-cotton, MOF-cotton, untreated cotton), and the interaction term. This ANOVA resulted in an F-Ratio of 24.78 and a probability of a greater F of <0.0001. This indicates significant differences for the effects (substrate type, reaction time, and the interaction term) tested with regard to the amount of methyl parathion removed (Table 4.3). Substrate type had the most significant effect on the removal of methyl parathion, followed by time and the cross between substrate type and time.

More specifically, the post-hoc mean comparisons with a Tukey correction indicated differences between each experiment based on the interaction term of substrate type and time (Table 4.4). From this analysis, it can be seen that regardless of time, the MOF-cotton and the untreated cotton fabric samples were not significantly different from one another. Alternatively, as time increases, the POM-MOF-cotton samples differ with reaction time after 2h. For example, there is a significant difference between the amount of methyl parathion removed from solution with the 0.5 h and 24 h POM-MOF-cotton samples. Also, comparing all specimen types at 0.5 h and again at 1 h, there is no significant difference in the amount of methyl parathion removed by the POM-MOF-cotton, MOF-cotton, or untreated cotton for each time. However, after 2, 12, and 24 h the POM-MOF-cotton samples remove significantly more methyl parathion than either the MOF-cotton or untreated cotton. The POM-MOF-cotton removed more methyl parathion with increased time.

Table 4.3. Result from effect tests related to the ANOVA performed for the removal of methyl parathion based on substrate type, reaction time, and interaction term of these two effects.

Effect	**F-Ratio**	**Prob > F**
Whole Model	24.78	<0.0001
Substrate Type	54.53	<0.0001
Time	8.54	0.0048
Interaction between Substrate Type and Time	3.17	0.0484

Table 4.4. Results from the post hoc mean comparisons with a Tukey correction showing the interaction between time and substrate type. Data interaction points not connected by the same letter are significantly different.

Sample Type	**Time (h)**					
	0.5	**1**	**2**	**6**	**12**	**24**
POM-MOF-cotton	BCD	ABCD	AB	ABC	AB	A
MOF-cotton	D	D	D	D	D	CD
Untreated cotton	D	D	D	CD	D	CD

4.5. Discussion

Visual observation of the telling blue color of Cu (II)[53] confirmed the incorporation of copper for both MOF-cotton and POM-MOF-cotton (Figure 4.1). The darker color of POM-MOF-cotton in comparison to MOF-cotton likely indicated that there was more copper in the POM-MOF-cotton sample, which was confirmed with the ICP-AES data (Table 4.1). The significant washing of these materials after self-assembly of the microstructures to ensure that any unattached reactants were removed would suggest that the MOF and the POM-MOF structures are bonded to the cellulose polymers as previously reported[54]. Based on these initial results, further characterization was done to further substantiate the assembly of MOF-199 particles and confirm the incorporation of the POM within the POM-MOF-cotton.

The crystal structures observed on the fiber surfaces by FE-SEM indicated that it is likely that MOF and POM-MOF were successfully assembled on the cotton fibers (Figure 4.2). The morphologies of these assembled crystals in the POM-MOF-cotton and MOF-cotton are similar to those previously reported for MOF structure on cotton fibers[53]. The octahedral shape of the POM-MOF and MOF crystals agrees with the cubic crystal system with a Fm-3m space group previously reported in the literature for MOF-199[38,39,55]. Self-assembly of the microstructures is further supported by the IR chemical analysis (Figure 4.3) and X-ray diffraction (Figure 4.4). The main peaks of the MOF-199 IR spectra matched with those observed in both POM-MOF-cotton and MOF-cotton. Similarly, the XRD peaks of MOF-199 are observed for both POM-MOF-cotton and MOF-cotton, and they are in agreement with those reported in the literature[38,39]. Additionally, since the POM XRD peaks were not observed in the

POM-MOF-cotton specimen, the POM is not in a crystalline form in this specimen. This is expected since each POM molecule is isolated within a MOF cage and therefore is unable to crystalize. Also, the x-ray diffraction patterns for the cotton and carboxymethylated cotton are in agreement with those found in the literature for cellulose and carboxymethylated cellulose[56,57]. In conjunction, these characterization results show that the MOF was successfully self-assembled on the fiber for both MOF-cotton and POM-MOF-cotton and that there is likely no crystalline POM in the samples.

Presence of the copper L_α adsorption edge in X-ray energy dispersive analysis supports that the MOF structure is likely assembled on the fibers for both the POM-cotton and POM-MOF-cotton, while the presence of the tungsten M_α adsorption edge in the POM-MOF-cotton indicates that the POM was successfully incorporated into the MOF structure. Based on the known chemical structures of the MOF [$Cu_3(C_9H_3O_6)_2$] and POM [$K_5CuPW_{11}O_{39}$], copper should be present in both the MOF and POM, where as tungsten should only be present in the POM. Thus, POM-MOF-cotton specimens should have both copper and tungsten while the MOF-cotton should have only copper, which is in agreement with the X-ray analysis.

To further confirm incorporation of the POM into the MOF structure, quantification of the amount of copper and tungsten present in the specimen was completed with ICP-AES (Table 4.1). The ICP-AES data showed a significantly higher weight percent of tungsten in POM-MOF-cotton sample in comparison to the controls: MOF-cotton and untreated cotton. From these elemental weight percentages of copper and tungsten (Table 4.1), weight percent of MOF and POM were calculated

(Table 4.5). These data show much more MOF in the POM-MOF-cotton than in the MOF-cotton, which agrees with the observation of microstructures for the POM-MOF-cotton that are on average 3 times larger than those on the MOF-cotton (Section 4.4.2). Additionally, the intensities of the MOF peaks in the IR and the XRD pattern indicate that less MOF assembled on the MOF-cotton than the POM-MOF-cotton. It is possible that under the experimental condition using solvent the system developed, the POM promotes the self-assembly of the POM-MOF microstructure.

Table 4.5. Calculated weight % of POM and MOF in POM-MOF-cotton and MOF-cotton fabric.

Sample	**MOF (wt %)**	**POM (wt%)**
POM-MOF-cotton	4.0	0.6
MOF-cotton	2.7	0.0

The performance data (Section 4.4.8) also indicated that the POM was present in the assembled MOF structure. It is clear that substrate type played a significant role in the removal of methyl parathion since the POM-MOF-cotton removed significantly more methyl parathion from the test solution than the MOF-cotton and untreated cotton. Both MOF-cotton and untreated cotton removed similar amount of methyl parathion with most removal occurring within the first 2 h. After 2 h or more, the POM-MOF-cotton samples removed more methyl parathion than the untreated cotton or the MOF-cotton (Table 4.4, Figure 4.6). This shows the activity of the POM incorporated in the POM-MOF-cotton indicating self-decontaminating properties based on the POM-MOF performance in the literature[39] leading to potential utility as materials for protective clothing.

However, to make sure the results of this performance data is not related to the differing amounts of MOF in the POM-MOF-Cotton and the MOF-Cotton, the performance data was normalized to the amount of MOF from Table 4.5. The average sample weight of the POM-MOF-Cotton samples was 24.3 mg, then multiplied by 4 wt% results in 0.97 mg MOF per sample. The average sample weight of the MOF-Cotton samples was 23.1 mg, then multiplied by 2.7 wt% results in 0.62 mg MOF per sample. Figure 3.7 shows the removed amount of methyl parathion for each sample type (mg) divided by the amount of MOF per sample (mg) over the active time range of 0 - 2 h shown previously.

ANOVA testing was completed using three different model effects, which were reaction time (0.5 - 24 h), substrate type (POM-MOF-cotton or MOF-cotton), and the interaction term. This ANOVA resulted in an F-Ratio of 3.41 and a

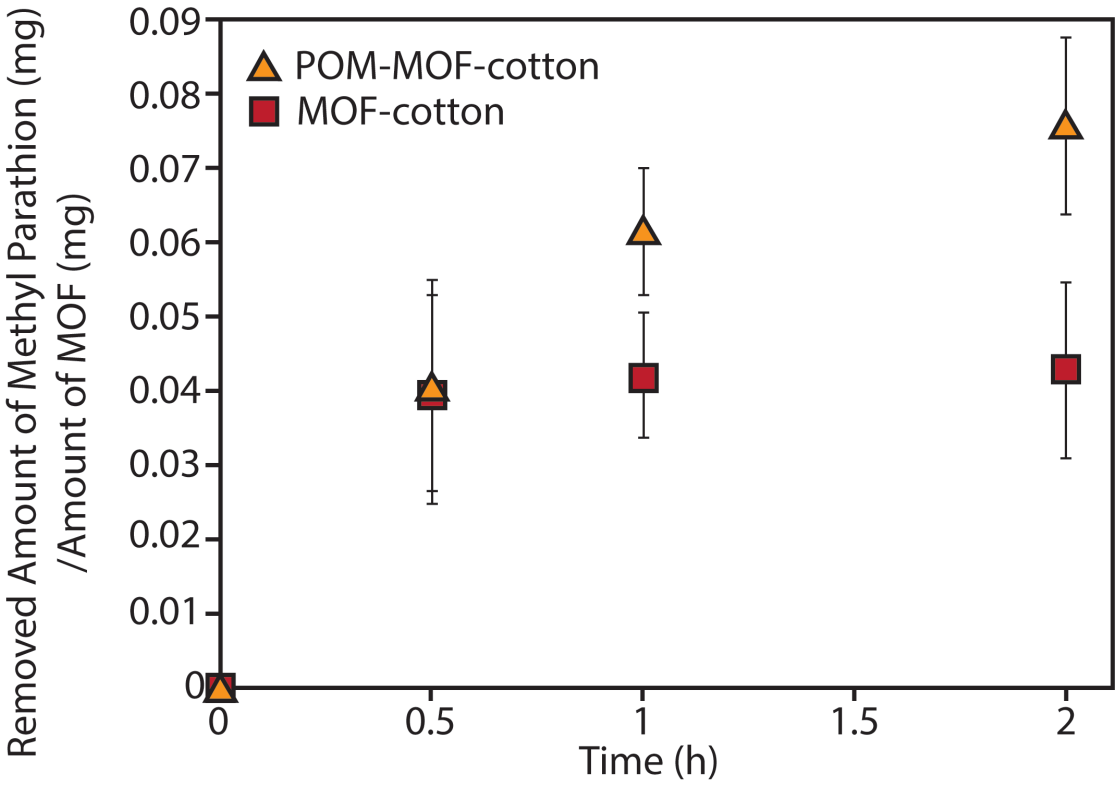

Figure 4.7. Removed amount of methyl parathion (mg) divided by amount of MOF (mg) over time for the two different substrate types (POM-MOF-cotton, MOF-cotton). Error bars indicate the standard deviation in both directions.

probability of a greater F of 0.0026. This indicates significant differences for the effects (substrate type, reaction time, and the interaction term) tested with regard to the amount of methyl parathion removed normalized to MOF amount (Table 4.6). Substrate type had a significant effect on the removal of methyl parathion, meaning there are still significant differences in the amount of methyl parathion removal after normalizing for amount of MOF. However, with MOF amount normalization time and the interaction term between substrate type and time were no longer significant to the 95% confidence level.

More specifically, the post-hoc mean comparisons with Student's t-tests indicated differences between each experiment based on the interaction term of substrate type and time (Table 4.7). From this analysis, it can be seen that regardless of time, the MOF-cotton fabric samples were still not significantly different from one another after normalization to amount of MOF. Alternatively, as time increases, the POM-MOF-cotton samples still show differences in the amount of methyl parathion removed from solution. For example, there is a significant difference between the amount of methyl parathion removed from solution with the 0.5 h and 2 h POM-MOF-cotton samples. However, there is now no significant difference between any of the POM-MOF-Cotton sample between 1h – 24h, further indicating that these materials remove the most methyl parathion before 2h. Also, after 2 - 24 h the POM-MOF-cotton samples still remove significantly more methyl parathion than the MOF-cotton after normalization.

Table 4.6. Result from effect tests related to the ANOVA performed for the removal of methyl parathion per amount of MOF based on substrate type, reaction time, and interaction term of these two effects.

Effect	**F-Ratio**	**Prob > F**
Whole Model	3.41	0.0026
Substrate Type	21.28	<0.0001
Time	2.31	0.0642
Interaction between Substrate Type and Time	0.93	0.4724

Table 4.7. Results from the post hoc mean comparisons with Student's t-tests showing the interaction between time and substrate type for removal of methyl parathion per amount of MOF. Data interaction points not connected by the same letter are significantly different.

Sample Type	**Time (h)**					
	0.5	**1**	**2**	**6**	**12**	**24**
POM-MOF-cotton	C	ABC	AB	AB	AB	A
MOF-cotton	C	C	C	C	C	BC

Moisture management is important in development of self-decontaminating materials and it affects thermal comfort of clothing. Some textile finishes reduce thermal comfort because of their hydrophobicity. Self-assembly of MOF and POM-MOF on the cotton fibers did not reduce its hydrophilicity (Table 4.2, TGA weight loss data after heating). Any water adsorption that may have been lost due to removal of a hydroxyl group is replaced by the addition of the open Cu(II) metal sites (Figure 4.8). The addition of the POM-MOF or MOF to the cotton did not affect the water adsorption properties; thus, thermal comfort of these protective materials will likely to be similar to untreated cotton.

Evaluating performance of these materials for use in protective clothing was a main concern for this research. It is important that protective clothing materials work in a timely fashion and maintain or improve thermal comfort. The POM-MOF-cotton samples demonstrated 2.75 times more methyl parathion removal compared to the MOF-cotton or untreated cotton (Figure 4.5). Given that no degradation products were observed in the hexane solution, it was concluded that degradation products were either adsorbed into the surrounding MOF pores or the methyl parathion was completely mineralized by the POM.

Based on the literature results indicating oxidation as the main method of degradation of toxins with the POM-MOF material[39], it is believed that self-decontaminating oxidation is also occurring when the POM-MOF is attached to the cotton. This potentially explains the increased removal of methyl parathion by the POM-MOF-cotton in comparison to the MOF-cotton samples. However, this is not shown conclusively by the data in this experiment. The maximum removal of methyl

parathion that occurs at about 2 hours is likely due to the clogging of the MOF cages with either methyl parathion or its degradation products. This theoretically blocks more methyl parathion from reaching the POM thereby hindering methyl parathion removal and possible degradation. This behavior of the POM-MOF materials was also proposed in the literature[39]. The probable self-decontaminating oxidation of methyl parathion by the POM in conjunction with the adsorption properties of the MOF when immobilized on a fabric is highly beneficial for use in protective clothing.

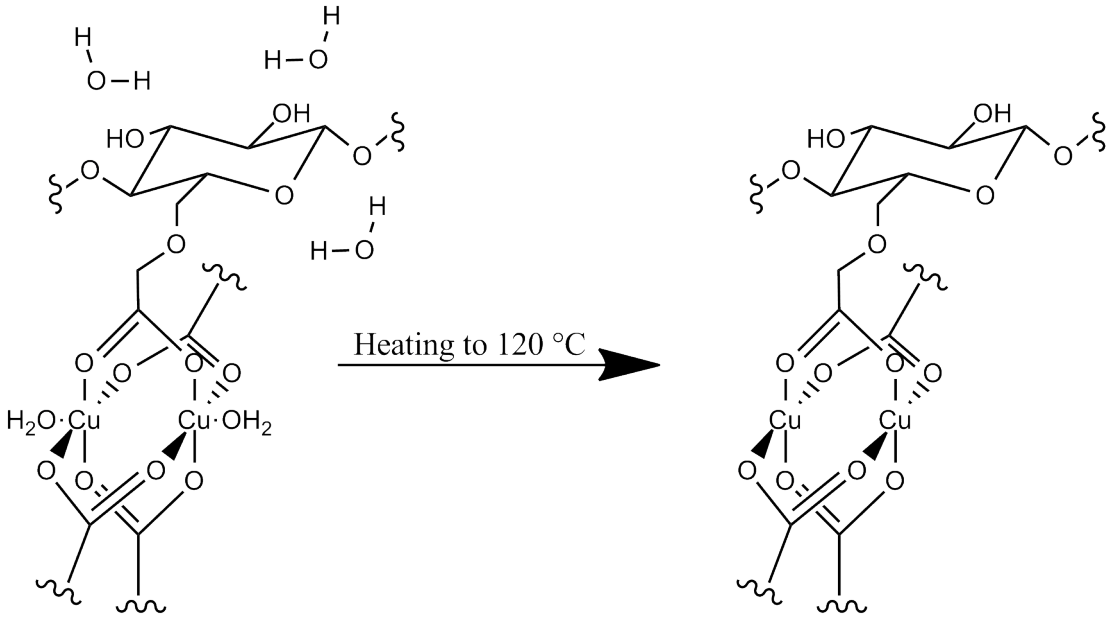

Figure 4.8. Water adsorption in MOF-cotton and POM-MOF-cotton samples and the effect of heating to 120 °C.

4.6. Conclusions

A method was developed to successfully assemble POM-MOF crystals on a cellulose substrate. Both MOF and POM-MOF structures were found to self-assemble on the fiber surface. These microstructures had all the characteristics of MOF-199 based on IR, XRD, FE-SEM analysis. POM was effectively incorporated into this MOF structure based on the X-ray microanalysis, elemental weight percent analysis, and performance data. In addition to the synergistic effects between the POM and the MOF reported previously[39], it was observed that they are also effective when assembled on the cellulose substrate. By incorporating the POM into the MOF-199 structure on the cotton fibers, methyl parathion removal was 2.75 times that of the MOF-cotton samples after 2 h indicating probable self-decontamination by oxidation. This adsorbent, self-decontaminating material is ideal for protective clothing. In addition, the hydrophilicity of the cellulosic material was maintained after assembly of the POM-MOF microstructures on the cotton, which is important for maintenance of thermal comfort.

4.7. Acknowledgements

Craig Hill and Zhen Luo are acknowledged for providing the polyoxometalate: $K_5[CuPW_{11}O_{39}]$. This research was funded through grants from the Cornell Agricultural Experiment Station, North Central Regional Research Project NC 170 federal formula funds, Project NYC329801 received from Cooperative State Research, Education, and Extension Service, U.S. Department of Agriculture; College of Human Ecology; Department of Fiber Science & Apparel Design; and the American Association of Textile Chemists and Colorists. This work made use of the Cornell

Center for Materials Research Shared Facilities, which are supported through the NSF MRSEC program (DMR-1120296).

4.8. REFERENCES

(1) Banks, K. E.; Hunter, D. H.; Wachal, D. J. *Environ. Int.* **2005**, 31, 351–356.

(2) Wilcox, D. E. *Chem. Rev.* **1996**, 96, 2435–2458.

(3) Vlyssides, A.; Barampouti, E. M.; Mai, S.; Arapoglou, D.; Kotronarou, A. *Environ. Sci. Technol.* **2004**, 38, 6125–6131.

(4) Kolinko, P. A.; Kozlov, D. V. *Environ. Sci. Technol.* **2008**, 42, 4350–4355.

(5) Kim, D. B.; Gweon, B.; Moon, S. Y.; Choe, W. *Curr. Appl. Phys.* **2009**, 9, 1093–1096.

(6) Zuo, G. M.; Cheng, Z. X.; Li, G. W.; Shi, W. P.; Miao, T. *Chem. Eng. J.* **2007**, 128, 135–140.

(7) Lange, L. E.; Obendorf, S. K. *Arch. Environ. Con. Tox.* **2012,** 62(2), 185-194.

(8) Dai, K.; Peng, T. Y.; Chen, H.; Liu, J.; Zan, L. *Environ. Sci. Technol.* **2009**, 43, 1540–1545.

(9) Wagner, G. W.; Bartram, P. W.; Koper, O; Klabunde, K. J. *J. Phys. Chem. B* **1999**, 103, 3225–3228.

(10) Wagner, G. W.; Procell, L. R.; O'Connor, R. J.; Munavalli, S.; Carnes, C. L.; Kapoor, P. N.; Klabunde, K. J. *J. Am. Chem. Soc.* **2001**, 123, 1636–1644.

(11) Wagner, G. W.; Procell, L. R.; Munavalli, S. *J. Phys. Chem. C* **2007**, 111, 17564–17569.

(12) Mahato, T.H.; Prasad, G.K.; Singh, B.; Acharya, J.; Srivastava, A.R.; Vijayaraghavan, R. *J. Hazard. Mater.* **2009**, 165, 928–932.

(13) Panayotov, D. A.; Morris, J. R. *J. Phys. Chem. C* **2008**, 112, 7496–7502.

(14) Columbus, I.; Waysbort, D.; Shmueli, L.; Nir, I.; Kaplan, D. *Environ. Sci.*

Technol. **2006**, 40, 3952–3958.

(15) Bromberg, L.; Schreuder-Gibson, H.; Creasy, W. R.; McGarvey, D. J.; Fry, R. A.; Hatton, T. A. *Ind. Eng. Chem. Res.* **2009**, 48, 1650–1659.

(16) Gomes, D. E. B.; Lins, R. D.; Pascutti, P. G.; Lei, C. H.; Soares, T. A. *J. Phys. Chem. B* **2010**, 114, 531–540.

(17) Seger, M. R.; Maciel, G. E. *Environ. Sci. Technol.* **2006**, 40, 797–802.

(18) Seger, M. R.; Maciel, G. E. *Environ. Sci. Technol.* **2006,** 40, 552-558.

(19) Seger, M. R.; Maciel, G. E. *Environ. Sci. Technol.* **2006**, 40, 791–796.

(20) Fei, X; Sun, G. *Ind. Eng. Chem. Res.* **2009**, 48, 5604–5609.

(21) Knagge, K.; Johnson, M.; Grassian, V. H.; Larsen, S. C. *Langmuir* **2006**, 22, 11077–11084.

(22) Lange, L. E.; Ochanda, F. O.; Obendorf, S. K.; Hinestroza, J. P. *Fiber Polym.* **2013,** accepted.

(23) Britt, D.; Furukawa, H.; Wang, B.; Glover, T. G.; Yaghi, O. M. *P. Natl. Acad. Sci. USA* **2009**, 106 (49), 20637-20640.

(24) Britt, D.; Tranchemontagne, D.; Yaghi, O.M. *P. Natl. Acad. Sci. USA* **2009**, 105 (33), 11623-11627.

(25) Furukawa, H.; Yaghi, O. M. *J. Am. Chem. Soc.* **2009**, 131, 8875-8883.

(26) Eddaoudi, M.; Kim, J.; Rosi, N.; Vodak, D.; Wachter, J.; O'Keeffe, M.; Yaghi, O. M. *Science* **2002**, 295, 469–472.

(27) Bordiga, S.; Regli, L.; Bonino, F.; Groppo, E.; Lamberti, C.; Xiao, B.; Wheatley, P. S.; Morris, R. E.; Zecchina, A. *Phys. Chem. Chem. Phys.* **2007**, 9, 2676-2685.

(28) Prestipino, C.; Regli, L.; Vitillo, J. G.; Bonino, F.; Damin, A.; Lamberti, C.; Zecchina, A.; Solari, P. L.; Kongshaug, K. O.; Bordiga, S. *Chem. Mater.* **2006**, 18, 1337-1346.

(29) Alaerts, L.; Wahlen, J.; Jacobs, P. A.; Vos, D. E. D. *Chem. Commun.* **2008,** 1727.

(30) Corma, A.; García, H.; Llabres i Xamena, F. X. *Chem. Rev.* **2010,** 110, 4606.

(31) Ma, L.; Abney, C.; Lin,W. *Chem.Soc.Rev.* **2009,** 38, 1248.

(32) Seo,J.S.;Whang,D.;Lee,H.;Jun,S.I.;Oh,J.;Jeon,Y.J.;Kim, K. *Nature* **2000,** 404, 982.

(33) Lee, J. Y.; Farha, O. K.; Roberts, J.; Scheidt, K. A.; Nguyen, S. B. T.; Hupp, J. T. *Chem. Soc. Rev.* **2009,** 38, 1450.

(34) Uemura, T.; Yanai, N.; Kitagawa, S. *Chem. Soc. Rev.* **2009,** 38, 1228.

(35) Wang, S.; Li, L.; Zhang, J.; Yuan, X.; Su, C.-Y. *J. Mater. Chem.* **2011,** 21, 7098.

(36) Ranocchiari, M.; van Bokhoven, J. A. *Phys. Chem. Chem. Phys.* **2011,** 13, 6388-6396.

(37) Schlichte, K.; Kratzke, T.; Kaskel, S. *Microporous Mesoporous Mater.* **2004,** 73, 81-88.

(38) Chui, S. S. Y.; Lo, S. M. F.; Charmant, J. P. H.; Orpen, A. G.; Williams, I. D. *Science* **1999,** 283, 1148.

(39) Song, J.; Luo, Z.; Furakawa, H.; Yaghi, O. M.; Hardcastle, K. I.; Hill, C. L. *J. Am. Chem. Soc.* **2011,** 133, 16839-16846.

(40) Guo, W.; Luo, Z.; Song, J.; Zhu, G.; Zhao, C.; Lv, H.; Vickers, J. W.; Geletii,

Y. V.; Djamaladdin, G. M.; Hill, C. L. (2012) Multi-electron Transfer Catalysts for Air-Based Organic Oxidations and Water Oxidation. In *Complexity in Chemistry and Beyond: Interplay Theory and Experiment.* (pp. 229-242) NATO Science for Peace and Security Series B: Physics and Biophysics.

(41) Hill, C. L.; Prosser-McCartha, C. M. *Coord Chem Rev* **1995**, 143, 407.

(42) Neumann, R. *Prog Inorg Chem* **1998,** 47, 317.

(43) Mizuno, N.; Misono, M. *Chem Rev* **1998,** 98, 199.

(44) Okuhara, T.; Mizuno, N.; Misono, M. *Appl Catal A* **2001,** 222, 63.

(45) Nakagawa, Y.; Kamata, K.; Kotani, M.; Yamaguchi, K.; Mizuno, N. *Angew Chem Int Ed* **2005,** 44, 5136.

(46) Juan-Alcañiz, J.; Gascon, J.; Kapteijn, F. *J Mater Chem* **2012**, 22, 10102.

(47) Maksimchuk, N.V.; Timofeeva, M. N.; Melgunov, M. S.; Shmakov, A. N.; Chesalov, Y. A.; Dybtsev, D. N.; Fedin, V. P.; Kholdeeva, O. A. *J Catal* **2008,** 257, 315.

(48) Maksimchuk, N. V.; Kovalenko, K. A.; Arzumanov, S. S.; Chesalov, Y. A.; Melgunov, M. S.; Stepanov, A. G.; Fedin, V. P.; Kholdeeva, O. A. *Inorg Chem* **2010,** 49, 2920.

(49) Juan-Alcañiz, J.; Ramos-Fernandez, E. V.; Lafont, U.; Gascon, J.; Kapteijn, F. *J Catal* **2010,** 269, 229.

(50) Juan-Alcañiz, J.; Goesten, M.; Martinez-Joaristi, A.; Stavitski, E.; Petukhov, A. V.; Gascon, J.; Kapteijn, F. *Chem Commun* **2011,** 47, 8578.

(51) Kim, J.; Yun, S.; Ounaies, Z. *Macromolecules* **2006,** 39, 4202–4206.

(52) Wang, Z.; Hauser, P. J.; Laine, J.; Rojas, O. J. *J. Adhes. Sci. Technol*. **2011,** 25, 643-660.

(53) da Silva Pinto, M.; Sierra-Avila, C. A.; Hinestroza, J. P. *Cellulose.* **2012,** 19, 1771-1779.

(54) Tranchemontagne, D. J.; Hunt, J. R.; Yaghi, O. M. *Tetrahedron* **2008,** 64, 8553-8557.

(55) Schlesinger, M.; Schulze, S.; Hietschold, M.; Mehring, M. *Microporous Mesoporous Mater*. **2010,** 132, 121-127.

(56) Bhandari, P. N.; Jones, D. D.; Hanna, M. A. *Carbohydrate Polymers*. **2012,** 87, 2246-2254.

(57) Vilela, C.; Freire, C. S. R.; Marques, P. A. A. P.; Trindade, T.; Neto, C. P.; Fardim, P. *Carbohydrate Polymers*. **2010,** 79, 1150-1156.

CHAPTER 5

CONCLUSIONS AND FUTURE WORK

The adsorption and degradation of methyl parathion, an organophosphate, with Cu-BTC metal-organic framework (MOF-199), and later in conjunction with a polyoxometalate, were investigated in multiple fibrous systems. By immobilizing MOF particles in a fibrous system, functionality was added to the fibers. This allowed for the MOF particles to be in a workable and flexible substrate. The combination of the POM and MOF on the surface of fibers was found to be the most promising system studied for potential uses in protective clothing and filtration media. The POM-MOF-cotton sample is promising because the combination of the probable self-decontaminating oxidation by the POM in conjunction with the adsorption properties of the MOF when immobilized on a fabric is highly beneficial for use in protective clothing. Based on this, further experiments should be completed to optimize this specific system.

The literature results indicate that oxidation is the main method of toxin degradation by the POM-MOF material. However, the presented research did not explore the degradation products observed with the POM-MOF-cotton material. Therefore, it would be beneficial to determine methyl parathion degradation products present in the POM-MOF-cotton specimen by utilizing ^{31}P solid-state NMR and solvent extractions to theoretically confirm the mechanism of methyl parathion removal, as not only adsorption, but as oxidative degradation as well.

One of the main criticisms of this work is that many chemical warfare agents

are gaseous and this study focused on liquid solutions of the pesticide. Therefore, it would be very interesting to test the POM-MOF-cotton specimen with a gaseous target compound. Determining the differences in the performance of POM-MOF-cotton specimen when challenged with a gas versus a liquid could be a very interesting study.

It would also be of interest to increase the amount of MOF cages occupied by POM to increase probable catalysis and degradation of methyl parathion. This would require altering the ratios of POM to MOF building blocks and likely the solvent system as well. I would be interesting to figure out if there is a maximum amount of POM that can be encapsulated in the MOF cages before performance begins to be hindered.

Growing the POM-MOF material on fibers other than cotton, such as nylon or potentially a polyolefin, is another project of interest. Using a plasma or UV surface treatment could create sites for POM-MOF crystal growth on a polyolefin. Growing the POM-MOF on a larger variety of fibers increases the possible applications of the developed materials. Also, other more hydrophobic fibers, such as polyolefins, could potentially experience a significant increase in hydrophilicity with the addition of the MOF and POM.

Overall, this dissertation showed that MOF-199 enmeshed in PAN fibers had the ability to remove methyl parathion from solution. It was also determined that MOF-199 itself has the ability to degrade methyl parathion, but it takes weeks to months for any significant degradation of methyl parathion to occur. This timeframe is far to slow for effective use in protective clothing. Therefore, by encapsulating the POM material within the MOF-199 cages, the goal was to reduce the amount of time

necessary to adsorb and theoretically degrade methyl parathion. Increased removal of methyl parathion by the POM-MOF-cotton sample after 2 h indicates that the POM makes a difference. Once further testing and optimization discussed above is complete, the POM-MOF-cotton could ideally be used as a scavenger material in a layered protective fabric system to provide protection to humans from dermal absorption of toxins.